



University of Dundee

Ethanolaminephosphate cytidyltransferase is essential for survival, lipid homeostasis and stress tolerance in *Leishmania major*

Basu, Somrita; Pawlowic, Mattie; Hsu, Fong-Fu; Thomas, Geoff; Zhang, Kai

DOI:
[10.1101/2023.01.10.523530](https://doi.org/10.1101/2023.01.10.523530)

Publication date:
2023

Licence:
CC BY

Document Version
Publisher's PDF, also known as Version of record

[Link to publication in Discovery Research Portal](#)

Citation for published version (APA):
Basu, S., Pawlowic, M., Hsu, F-F., Thomas, G., & Zhang, K. (2023). *Ethanolaminephosphate cytidyltransferase is essential for survival, lipid homeostasis and stress tolerance in Leishmania major*. BioRxiv. <https://doi.org/10.1101/2023.01.10.523530>

General rights

Copyright and moral rights for the publications made accessible in Discovery Research Portal are retained by the authors and/or other copyright owners and it is a condition of accessing publications that users recognise and abide by the legal requirements associated with these rights.

- Users may download and print one copy of any publication from Discovery Research Portal for the purpose of private study or research.
- You may not further distribute the material or use it for any profit-making activity or commercial gain.
- You may freely distribute the URL identifying the publication in the public portal.

Take down policy

If you believe that this document breaches copyright please contact us providing details, and we will remove access to the work immediately and investigate your claim.

1 **Ethanolaminephosphate cytidyltransferase is essential for survival, lipid**
2 **homeostasis and stress tolerance in *Leishmania major***

3
4 Somrita Basu¹, Mattie Pawlowic², Fong-Fu Hsu³, Geoff Thomas¹, and Kai Zhang^{1*}

5
6 ¹Department of Biological Sciences, Texas Tech University, Lubbock, TX 79409, USA.

7 ²Wellcome Centre for Anti-Infectives Research (WCAIR), Division of Biological Chemistry and
8 Drug Discovery, School of Life Sciences, University of Dundee, Dundee, DD1 5EH, UK.

9 ³Mass Spectrometry Resource, Division of Endocrinology, Diabetes, Metabolism, and Lipid
10 Research, Department of Internal Medicine, Washington University School of Medicine, 660S.
11 Euclid Ave., Saint Louis, MO 63110, USA.

12
13 *Corresponding author: Kai Zhang, Department of Biological Sciences, Texas Tech University,
14 Lubbock, TX 79409, USA. Tel: 806-834-0550; Email: kai.zhang@ttu.edu.

15
16 Short title: *De novo* PE synthesis is essential in *Leishmania*

17

18

19

20

21

22

23

24 **ABSTRACT**

25 Glycerophospholipids including phosphatidylethanolamine (PE) and phosphatidylcholine
26 (PC) are vital components of biological membranes. Trypanosomatid parasites of the genus
27 *Leishmania* can acquire PE and PC via *de novo* synthesis and the uptake/remodeling of host
28 lipids. In this study, we investigated the ethanolaminephosphate cytidyltransferase (EPCT) in
29 *Leishmania major*, which is the causative agent for cutaneous leishmaniasis. EPCT is a key
30 enzyme in the ethanolamine branch of the Kennedy pathway which is responsible for the *de novo*
31 synthesis of PE. Our results demonstrate that *L. major* EPCT is a cytosolic protein capable of
32 catalyzing the formation of CDP-ethanolamine from ethanolamine-phosphate and cytidine
33 triphosphate. Genetic manipulation experiments indicate that EPCT is essential in both the
34 promastigote and amastigote stages of *L. major* as the chromosomal null mutants cannot survive
35 without the episomal expression of EPCT. This differs from our previous findings on the choline
36 branch of the Kennedy pathway (responsible for PC synthesis) which is required only in
37 promastigotes but not amastigotes. While episomal EPCT expression does not affect
38 promastigote proliferation under normal conditions, it leads to reduced production of
39 ethanolamine plasmalogen or plasmenylethanolamine, the dominant PE subtype in *Leishmania*.
40 In addition, parasites with episomal EPCT exhibit heightened sensitivity to acidic pH and
41 starvation stress, and significant reduction in virulence. In summary, our investigation
42 demonstrates that proper regulation of EPCT expression is crucial for PE synthesis, stress
43 response, and survival of *Leishmania* parasites throughout their life cycle.

44 **AUTHOR SUMMARY**

45 In nature, *Leishmania* parasites alternate between fast replicating, extracellular
46 promastigotes in sand fly gut and slow growing, intracellular amastigotes in macrophages.
47 Previous studies suggest that promastigotes acquire most of their lipids via *de novo* synthesis
48 whereas amastigotes rely on the uptake and remodeling of host lipids. Here we investigated the
49 function of ethanolaminephosphate cytidyltransferase (EPCT) which catalyzes a key step in the
50 *de novo* synthesis of phosphatidylethanolamine (PE) in *Leishmania major*. Results showed that
51 EPCT is indispensable for both promastigotes and amastigotes, indicating that *de novo* PE
52 synthesis is still needed at certain capacity for the intracellular form of *Leishmania* parasites. In
53 addition, elevated EPCT expression alters overall PE synthesis and compromises parasite's
54 tolerance to adverse conditions and is deleterious to the growth of intracellular amastigotes.
55 These findings provide new insight into how *Leishmania* acquire essential phospholipids and
56 how disturbance of lipid metabolism can impact parasite fitness.

57 INTRODUCTION

58 Protozoan parasites of the genus *Leishmania* are transmitted through the bite of
59 hematophagous sand flies. During their life cycle, *Leishmania* parasites alternate between
60 flagellated, extracellular promastigotes in sand fly midgut and non-flagellated, intracellular
61 amastigotes in mammalian macrophages. These parasites cause leishmaniasis which ranks
62 among the top ten neglected tropical diseases with 10-12 million people infected and 350 million
63 people at the risk of acquiring infection [1, 2]. Drugs for leishmaniasis are plagued with strong
64 toxicity, low efficacy, and high cost [3, 4]. To develop better treatment, it is necessary to gain
65 insights into how *Leishmania* acquire essential nutrients and proliferate in the harsh environment
66 in the vector host and mammalian host.

67 To sustain growth, *Leishmania* parasites must generate abundant amounts of lipids
68 including glycerophospholipids, sterols and sphingolipids. Phosphatidylethanolamine (PE) and
69 phosphatidylcholine (PC) are two common classes of glycerophospholipids. Besides being major
70 membrane constituents, PE and PC can function as precursors for several signaling molecules
71 and metabolic intermediates including lyso-phospholipids, phosphatidic acid, diacylglycerol, and
72 free fatty acids [5, 6]. In addition, PE contributes to the synthesis of GPI-anchored proteins
73 in trypanosomatid parasites by providing the ethanolamine phosphate bridge that links proteins
74 to glycan anchors [7]. PE is also involved in the formation of autophagosome during
75 differentiation and starvation in *Leishmania major* [8, 9] and the posttranslational modification
76 of eukaryotic elongation factor 1A in *T. brucei* [10].

77 For many eukaryotic cells, the majority of PE and PC are synthesized *de novo* via the
78 Kennedy pathway (Fig. 1) [11]. In *Leishmania*, the key metabolite ethanolamine phosphate
79 (EtN-P) is generated from of the sphingoid base metabolism or the phosphorylation of

80 ethanolamine (EtN) by ethanolamine kinase [12](Fig. 1). EtN-P is then conjugated to cytidine
81 triphosphate (CTP) to produce CDP-EtN and pyrophosphate by the enzyme
82 ethanolaminephosphate cytidyltransferase (EPCT) [13]. In the EtN branch of the Kennedy
83 pathway, through the activity of ethanolamine phosphotransferase (EPT), CDP-EtN is combined
84 with 1-alkyl-2-acyl-glycerol to generate plasmenylethanolamine (PME) or ethanolamine
85 plasmalogen, the dominant subtype of PE in *Leishmania* [14]. CDP-EtN can also be combined
86 with 1,2-diacylglycerol to form 1,2-diacyl-PE (a minor subtype of PE in *Leishmania*) by choline
87 ethanolamine phosphotransferase (CEPT) [15, 16]. A similar branch of the Kennedy pathway is
88 responsible for the *de novo* synthesis of PC (choline → choline-phosphate → CDP-choline →
89 PC), with CEPT catalyzing the last step of conjugating CDP-choline and diacylglycerol into PC
90 as a dual activity enzyme [16-18]. Besides the Kennedy pathway, PE may be generated from the
91 decarboxylation of phosphatidylserine (PS) in the mitochondria and PC may be generated from
92 the N-methylation of PE [19-21].

93 In addition to biosynthesis, *Leishmania* parasites (especially the intracellular amastigotes)
94 can take up and modify existing lipids to fulfill their needs [22-24]. For example, the enzyme
95 CEPT which is directly responsible for producing PC and diacyl-PE (Fig. 1) is essential for *L.*
96 *major* promastigotes in culture but is not required for the survival or proliferation of amastigotes
97 in mice [18]. While diacyl-PE is a minor lipid component in *Leishmania*, PC is highly abundant
98 in both promastigotes and amastigotes [25, 26]. These results argue that *de novo* PC synthesis is
99 required to generate large amount of lipids to support rapid parasite replication during the
100 promastigote stage (estimated doubling time: 6–8 hours in culture and 10–12 hours in sand fly)
101 [27, 28]. In contrast, intracellular amastigotes can acquire enough PC through the uptake and
102 remodeling of host lipids, which seems to fit their slow growing, metabolically quiescent state

103 (estimated doubling time: 60 hours) [29, 30]. Consistent with these findings, sphingolipid
104 analyses of *L. major* amastigotes revealed high levels of sphingomyelin which could not be
105 synthesized by *Leishmania* but was plentiful in mammalian cells [31]. Conversely, the
106 biosynthesis of parasite-specific sphingolipid, inositol phosphorylceramide (IPC), is fully
107 dispensable for *L. major* amastigotes [12, 31, 32]. Collectively, these data suggest that as
108 *Leishmania* transition from fast-replicating promastigotes to slow-growing amastigotes, they
109 undergo a metabolic switch from *de novo* synthesis to scavenge/remodeling to acquire their
110 lipids [24].

111 Despite of these findings, it is important to explore whether intracellular amastigotes
112 retain some capacity for *de novo* lipid synthesis. Our previous studies on the sterol biosynthetic
113 mutant *c14dm*⁻ suggest that is the case [33]. *L. major c14dm*⁻ mutants lack the sterol-14 α -
114 demethylase which catalyzes the removal of C-14 methyl group from sterol intermediates.
115 Promastigotes of *c14dm*⁻ are devoid of ergostane-type sterols (which are abundant in wild type
116 [WT] parasites) and accumulate 14-methyl sterol intermediates. However, lipid analyses of
117 lesion-derived amastigotes demonstrate that both WT and *c14dm*⁻ amastigotes contain
118 cholesterol (which must be taken from the host since *Leishmania* only synthesize ergostane-type
119 sterols) as their main sterol [33]. Parasite-specific sterols, i.e., ergostane-type sterols such as
120 ergosterol and 5-dehydroepisterol in WT amastigotes and C-14-methylated sterols in *c14dm*⁻
121 amastigotes are only detected at trace levels. Nonetheless, *c14dm*⁻ amastigotes show
122 significantly attenuated virulence and reduced growth in comparison to WT and *C14DM* add-
123 back amastigotes, suggesting that the residual amounts of endogenous sterols (which cannot be
124 scavenged from the host) play pivotal roles in amastigotes which may constitute the basis for
125 sterol biosynthetic inhibitors as anti-leishmaniasis drugs [33, 34].

126 In this study, we investigated the roles of EPCT (EC 2.7.7.14) which catalyzes the
127 conversion of EtN-P and CTP into CDP-EtN and pyrophosphate in the Kennedy pathway (Fig.
128 1). Our previous study on EPT in *L. major* revealed that EPT is mostly required for the synthesis
129 of PME but not diacyl PE or PC [14]. Disruption of EPCT, on the other hand, may have a much
130 more profound impact on the synthesis of PME, diacyl PE and PC (which can be generated from
131 diacyl PE via N-methylation) (Fig. 1). In mammalian cells, EPCT is considered as the rate
132 limiting enzyme in the EtN branch of the Kennedy pathway and a key regulator of PE synthesis
133 [35, 36]. Disruption of EPCT in mice leads to developmental defects and embryonic lethality
134 [37, 38]. Additional studies report EPCT heterozygous mice have increased diacylglycerol and
135 triacylglycerol in liver that resemble features of metabolic diseases, suggesting that EPCT is
136 involved in maintaining the homeostasis of neutral lipids as well [38, 39]. Based on these
137 findings, it is of interest to determine the roles of EPCT in *Leishmania* especially during the
138 disease-causing intracellular stage when parasites acquire most of their lipids via scavenging.
139 Our results indicate that EPCT is essential for the survival of both promastigotes and amastigotes
140 in *L. major*. In addition, the expression level of EPCT is crucial for stress tolerance, lipid
141 homeostasis and the synthesis of GPI-anchored proteins. These findings may inform the
142 development of new anti-*Leishmania* drugs.

143 RESULTS

144 Identification and functional verification of *L. major* EPCT

145 A putative *EPCT* gene was identified in the genome of *L. major* (Tritypdb: LmjF
146 32.0890) with synthetic orthologs in other *Leishmania* spp., *Trypanosoma brucei*, and
147 *Trypanosoma cruzi*. The predicted *L. major* EPCT protein consists of 402 amino acids and bears
148 35-42% identity to EPCTs from *Saccharomyces cerevisiae*, *Plasmodium falciparum*,
149 *Arabidopsis thaliana*, and *Homo sapiens* (Fig. S1).

150 To confirm its function, the *EPCT* open reading frame (ORF) was cloned into a pXG
151 plasmid (a high copy number protein expression vector) [40] and introduced into *L. major* wild
152 type parasites (WT) as WT+EPCT. When promastigote lysate from WT+EPCT was incubated
153 with [¹⁴C]-EtN-P and CTP for 20 minutes at room temperature, we detected a radiolabeled
154 product which exhibited similar mobility (retention factor) as pure CDP-EtN on thin layer
155 chromatography (TLC), suggesting it was [¹⁴C]-CDP-EtN (Fig. 2A and Fig. S2A). Radiolabeled
156 CDP-EtN was also observed when [¹⁴C]-EtN-P and CTP were incubated with mouse liver
157 homogenate, but not boiled lysates (Fig. 2A and Fig. S2B). We did not detect the formation of
158 [¹⁴C]-CDP-EtN using WT lysate, indicating that the basal level of EPCT activity in *L. major*
159 promastigotes was below the level of detection with this approach (Fig. 2A). To determine the
160 cellular localization of EPCT, a GFP-tagged EPCT was introduced into WT promastigotes as
161 WT+GFP-EPCT. As shown in Fig. 2B-C, GFP-EPCT was detected at the predicted molecular
162 weight of ~73 kDa and exhibited a cytoplasmic localization. In addition, WT+GFP-EPCT cells
163 displayed similar EPCT activity levels as WT+EPCT cells (Fig. 2A). Together, these findings
164 argue that *L. major* EPCT is a cytosolic enzyme capable of condensing EtN-P and CTP into
165 CDP-EtN.

166 **Chromosomal *EPCT*-null mutants cannot be generated without a complementing episome**

167 To determine whether *EPCT* is required for survival in *L. major*, we first attempted to
168 delete the two chromosomal *EPCT* alleles using the homologous recombination approach [41].
169 As demonstrated by Southern blot (Fig. S3A-B), we successfully replaced one *EPCT* allele with
170 the blasticidin resistance gene (*BSD*) using this approach and generated several heterozygous
171 *EPCT*^{+/-} clones. However, repeated attempts to delete the second *EPCT* allele failed to recover
172 any true knockouts (results from one attempt was shown in Fig. S3C-D), suggesting that a
173 different method is needed to generate chromosomal *EPCT*-null mutants.

174 We then adopted the complementing episome-assisted knockout approach that has been
175 used to study essential genes in *Leishmania* [42-44]. To do so, a pXNG4-*EPCT* plasmid
176 (complementing episome) containing genes for *EPCT*, green fluorescence protein (*GFP*),
177 nourseothricin resistance (*SAT*) and thymidine kinase (*TK*) was constructed and introduced into
178 *EPCT*^{+/-} parasites (*EPCT*^{+/-} +pXNG4-*EPCT*), followed by attempts to delete the second
179 chromosomal *EPCT* allele with the puromycin resistance gene (*PAC*) (Fig. S4). With this
180 approach, we were able to generate multiple clones showing successful replacement of
181 chromosomal *EPCT* with *BSD* and *PAC* (*epct*⁻ + pXNG4-*EPCT* in Fig. 3A-B and Fig. S4).
182 Southern blot with an *EPCT* ORF probe revealed high levels of pXNG4-*EPCT* plasmid (20-35
183 copies/cell) in these *epct*⁻ + pXNG4-*EPCT* parasites but no endogenous *EPCT* was detected (Fig.
184 3C-D and Fig. S4). Overexpression of *EPCT* from the pXNG4-*EPCT* plasmid did not have any
185 significant effect on promastigote replication under normal culture conditions (Fig. 3E).

186 ***EPCT* is essential for *L. major* promastigotes**

187 To evaluate the essentiality of *EPCT*, *EPCT*^{+/-} +pXNG4-*EPCT* and *epct*⁻ + pXNG4-
188 *EPCT* promastigotes were cultivated in the presence or absence of ganciclovir (GCV). Because

189 of the *TK* expression from pXNG4-EPCT, adding GCV would trigger premature termination of
190 DNA synthesis [42]. Thus, in the presence of GCV, parasites would favor the elimination of
191 pXNG4-EPCT (which can be tracked by monitoring GFP fluorescence level) during replication
192 to avoid toxicity, if the episome is dispensable [42]. As shown in Fig. 4A, after being cultivated
193 in the presence of GCV for 14 consecutive passages, those chromosomal *EPCT*-null
194 promastigotes still contained 60-74% of GFP-high cells, indicative of high pXNG4-EPCT
195 retention levels after prolonged negative selection. In contrast, the pXNG4-EPCT plasmid was
196 easily expelled from the *EPCT*^{+/-} +pXNG4-EPCT parasites after 8 passages in GCV (Fig. 4A),
197 suggesting that the remaining chromosomal *EPCT* allele made the episome expendable. Without
198 GCV, we detected a gradual loss of episome in the *EPCT*^{+/-} +pXNG4-EPCT but not *epct*⁻ +
199 pXNG4-EPCT parasites (Fig. 4A), again arguing that the episome is indispensable in those
200 chromosomal-null mutants. As controls, parasites grown in the presence of nourseothricin (the
201 positive selection) consistently retained 85-91% GFP-high cells (“+SAT” in Fig. 4A-C).

202 Our analysis showed that 25-38% of *epct*⁻ + pXNG4-EPCT parasites became GFP-low
203 after extended exposure to GCV (Fig. 4A and D). To examine whether these GFP-low cells were
204 episome-free or harbored altered episome with mutations in *TK* and/or *GFP*, they were separated
205 from GFP-high cells by fluorescence-activated cell sorting and individual clones were isolated
206 after serial dilution. Two such clones were analyzed by flow cytometry showing similar
207 percentages of GFP-high cells (70-74%) as the population prior to sorting (Fig. 4D-F),
208 suggesting that the GFP-low cells were only viable in the presence of GFP-high cells.
209 Additionally, quantitative PCR (qPCR) analyses were performed on these clones using primers
210 targeting the *GFP* region (to determine total plasmid copy number) and the *L. major* 28S rDNA
211 (to determine total parasite number). Results revealed ~8 copies of pXNG4-EPCT plasmid per

212 cell in the *epct*⁻+ pXNG4-EPCT GCV-treated clones, whereas the *EPCT*^{+/-}+ pXNG4-EPCT
213 clones isolated by the same process (GCV treatment → GFP-low sorting → serial dilution)
214 contained <0.01 copy per cell (Fig. S5A). We also sequenced the pXNG4-EPCT plasmid DNA
215 from GCV-treated *epct*⁻+ pXNG4-EPCT clones and did not find mutations in *TK*, *GFP* or
216 *EPCT*. Finally, we found a significant growth delay in GCV-treated *epct*⁻+ pXNG4-EPCT but
217 not *EPCT*^{+/-}+ pXNG4-EPCT promastigotes in comparison to control cells (Fig. S5B). This is
218 consistent with the episome retention in *epct*⁻+ pXNG4-EPCT which leads to GCV-induced
219 cytotoxicity. Together, these findings demonstrate the essential nature of EPCT in *L. major*
220 promastigotes.

221 **EPCT is indispensable for *L. major* amastigotes**

222 To investigate if EPCT is required for the survival of intracellular amastigotes, we
223 infected BALB/c mice in the footpad with stationary phase promastigotes. After infection, half
224 of the mice received daily GCV treatment, and the other half received equivalent amount of PBS
225 (control group) for 14 consecutive days as previously described [44]. No significant changes in
226 mouse body weight or movement were detected from GCV treatment (Fig. S6A). Mice infected
227 by WT and *EPCT*^{+/-} parasites exhibited equally rapid development of footpad lesions that
228 correlated with robust parasite replication, indicating that one chromosomal copy of *EPCT* is
229 sufficient for the mammalian stage (Fig. 5A-B). Importantly, mice infected by *EPCT*^{+/-}
230 +pXNG4-EPCT or *epct*⁻+ pXNG4-EPCT showed a 9-12-week delay in lesion development (Fig.
231 5A), and the delay was consistent with the significantly reduced parasite growth as determined
232 by limiting dilution assay and qPCR (Fig. 5B and Fig. S6B). While GCV treatment had little
233 impact on infections caused by WT, *EPCT*^{+/-}, or *EPCT*^{+/-}+ pXNG4-EPCT parasites, it caused
234 an additional 3-4-week delay in lesion progression for *epct*⁻+ pXNG4-EPCT (Fig. 5A-B),

235 suggesting that GCV-induced cytotoxicity is more significant in the chromosomal null mutants
236 than others.

237 To determine the pXNG4-EPCT copy number in amastigotes, we performed qPCR
238 analyses on genomic DNA extracted from lesion-derived amastigotes. The average plasmid copy
239 number per cell was revealed by dividing the total plasmid copy number with total parasite
240 number. As shown in Fig. 5C, *EPCT*^{+/-} +pXNG4-EPCT amastigotes contained 8-13 copies per
241 cell at week 4 post infection and that number gradually went down to 1.5-2.5 copies per cell by
242 week 14-20; and GCV treatment caused reduction in plasmid copy number as expected. The
243 reduction in plasmid copy number over time suggests that the episome is not required in
244 *EPCT*^{+/-} +pXNG4-EPCT amastigotes. In comparison, *epct*⁻ + pXNG4-EPCT amastigotes
245 maintained 15-30 plasmid copies per cell throughout the course of infection even with GCV
246 treatment (Fig. 5C). Thus, these chromosomal *EPCT*-null amastigotes must retain a high
247 episome level to survive which is consistent with their increased sensitivity to GCV (Fig. 5A-B),
248 Together, these data argue that EPCT is critically important for the survival of intracellular
249 amastigotes.

250 **EPCT overexpression leads to significantly attenuated virulence in mice**

251 Results from our mouse experiments suggest that elevated EPCT expression from
252 pXNG4-EPCT, a high copy number plasmid (Fig. 3C and Fig. 5C), may be responsible for the
253 delayed lesion progression and amastigote growth from *EPCT*^{+/-} +pXNG4-EPCT and *epct*⁻ +
254 pXNG4-EPCT promastigotes (Fig. 5 and Fig. S6). To test this hypothesis, we introduced
255 pXNG4-EPCT into WT parasites and the resulting WT +pXNG4-EPCT cells showed similar
256 infectivity in mice as *EPCT*^{+/-} +pXNG4-EPCT or *epct*⁻ + pXNG4-EPCT parasites (Fig. 5),
257 indicating that this plasmid can attenuate virulence in the WT background as well. In addition,

258 the *EPCT* gene was cloned into a pGEM vector along with its 5'- and 3'-flanking sequences (~1
259 Kb each) and the resulting pGEM-EPCT was introduced into *EPCT*^{+/-} parasites. Like cells with
260 pXNG4-EPCT, these *EPCT*^{+/-} + pGEM-EPCT parasites displayed significantly reduced
261 virulence and growth in BALB/c mice (Fig. S7), proving that these defects were caused by
262 EPCT overexpression and not restricted to the pXNG4 plasmid.

263 Like *EPCT*^{+/-} +pXNG4-EPCT, the episome copy number in WT +pXNG4-EPCT
264 amastigotes decreased from 14-16 per cell at week 4 post infection to 2-4 per cell in week 14-20
265 (Fig. 5C). Curiously, neither *EPCT*^{+/-} +pXNG4-EPCT amastigotes nor WT +pXNG4-EPCT
266 amastigotes could completely lose the episome like *EPCT*^{+/-} +pXNG4-EPCT promastigotes in
267 culture after GCV treatment (Fig. 4A and Fig. 5A). Our previous studies on farnesyl
268 pyrophosphate synthase (FPPS) and CEPT have demonstrated that heterozygous mutants of
269 those genes lost most of their respective episome (<0.2 copy per cell for *FPPS*^{+/-} +pXNG4-
270 FPPS and *CEPT*^{+/-} +pXNG4-CEPT) within 6 weeks post infection [18, 44]. It is possible that
271 the slow replication rates of *EPCT*^{+/-} +pXNG4-EPCT and WT +pXNG4-EPCT amastigotes
272 prevented complete plasmid loss.

273 In addition to plasmid copy number, we also examined EPCT transcript levels by reverse
274 transcription-qPCR using α -tubulin transcript as the internal standard (Fig. 6). For WT parasites,
275 EPCT mRNA level went down ~60% from promastigotes to amastigotes, consistent with the
276 relatively slow replication rate for amastigotes (Fig. 6A). As expected, the presence of pXNG4-
277 EPCT resulted in a 10-18-fold increase in EPCT mRNA levels (comparing to WT cells) during
278 the promastigote stage (Fig. 6B). While the overexpression was less pronounced during the
279 mammalian stage, we still observed a 2-8-fold increase in EPCT mRNA in *epct*⁻ + pXNG4-
280 EPCT amastigotes (week 14-20 post infection) in comparison to WT amastigotes (Fig. 6C).

281 From these findings, we conclude that while EPCT is essential, episome-induced EPCT
282 overexpression is detrimental to *L. major* growth during the mammalian stage.

283 **Changes in EPCT expression affects the syntheses of glycerophospholipids and GP63**

284 To examine if *EPCT* expression level affects phospholipid composition in *L. major*, total
285 lipids were extracted from stationary phase promastigotes and analyzed by electrospray
286 ionization mass spectrometry (ESI-MS). To detect PME and diacyl-PE, we used precursor ion
287 scan of m/z 196 in the negative ion mode and added 14:0/14:0-PE as a standard for quantitation
288 (Fig. 7). As shown in Fig. 7, EPCT-overexpressing cells (WT +pXNG4-EPCT, EPCT+/-
289 +pXNG4-EPCT and *epct*⁻+ pXNG4-EPCT) had 30-50% less PME (*p*18:0/18:2- and *p*18:0/18:1-
290 PE) relative to WT promastigotes. Meanwhile, the overall PME level in EPCT+/- was only
291 slightly less than WT (due to reduced level of *p*18:0/18:1-PE), and there was no significant
292 change in the abundance of diacyl-PE molecules (Fig. 7). Similar ESI-MS analyses were
293 performed to determine the levels of PC, phosphatidylinositol (PI), and IPC (the major
294 sphingolipid in *Leishmania*). As summarized in Fig. 8 and Fig. S8, *EPCT* half knockout
295 (EPCT+/-) or over-expression did not affect the composition of PC or IPC. Furthermore, *EPCT*
296 overexpressing cells had 20-30% less 18:0/18:1-PI, the most abundant type of PI in comparison
297 to WT cells (Fig. 9). We also detected a ~70% reduction in the level of a18:0/18:1-PI (an alkyl-
298 acyl PI) in WT+ pXNG4-*EPCT* parasites (Fig. 9). Collectively, these lipidomic analyses suggest
299 that proper regulation of *EPCT* expression is vital for the balanced synthesis of
300 glycerophospholipids.

301 Next, because PE and PI are involved in the biosynthesis of GP63 (a zinc-dependent,
302 GPI-anchored metalloprotease) and lipophosphoglycan (LPG), respectively, we examined
303 whether *EPCT* under- or over-expression could influence the production of these surface

304 glycoconjugates. Interestingly, immunofluorescence microscopy revealed a 4-5-fold reduction of
305 GP63 in EPCT^{+/-}, WT +pXNG4-EPCT, and EPCT^{+/-} +pXNG4-EPCT parasites and a nearly 8-
306 fold reduction in *epct*⁻ + pXNG4-EPCT (Fig. 10A and C). On the other hand, the cellular levels
307 of LPG were unaltered in EPCT mutant lines (Fig. 10B and D). These findings argue that EPCT
308 expression from its chromosomal locus are required for the proper synthesis of GP63.

309 **EPCT overexpression affects stress response**

310 To further explore how EPCT overexpression may compromise *L. major* virulence, we
311 examined the response of mutants to starvation, acidic pH and heat stress as tolerance to these
312 stress conditions are essential for parasite survival in the macrophage phagolysosome. Under
313 normal conditions (complete M199 medium, pH7.4, 27 °C), EPCT^{+/-} and overexpressors
314 proliferated at similar rates as WT promastigotes in log phase and exhibited good viability in
315 stationary phase (Fig. 3E and Fig. 11A). However, if cells were transferred to phosphate-
316 buffered saline (PBS, pH7.4) to test starvation tolerance, 50-60% of EPCT overexpressing cells
317 (WT+pXNG4-EPCT, EPCT^{+/-} +pXNG4-EPCT and *epct*⁻ + pXNG4-EPCT) died after 2-3 days
318 in comparison to <20% death for WT parasites (Fig. 11B). These overexpressors also showed a
319 24–48-hour growth delay if they were cultivated in a pH5.0 medium (Fig. 11D). In addition,
320 *epct*⁻ + pXNG4-EPCT parasites were slightly more sensitive to acidic stress (pH 5.0) and heat
321 (37 °C) than WT in the stationary phase (Fig. 11C and F). We did not detect any significant
322 difference in mitochondrial superoxide level between WT and EPCT mutants (Fig. S9). Whether
323 these defects are linked to the altered lipid contents in EPCT overexpressors remains to be
324 determined. Regardless, sensitivity to stress conditions likely contributes to their lack of
325 virulence.

326 DISCUSSION

327 Using a complementing episome assisted knockout approach coupled with negative
328 selection, we demonstrate that EPCT is indispensable throughout the life cycle in *L. major*. The
329 same method was applied to verify the essentiality of several genes in *Leishmania* [42-44]. With
330 EPCT being essential in both promastigotes and amastigotes, it is time to recognize EPCT as the
331 most important enzyme of the Kennedy pathway. This is in sharp contrast to cholinephosphate
332 cytidyltransferase (CPCT) which catalyzes the equivalent step in the choline branch of the
333 Kennedy pathway by combining choline phosphate and CTP into CDP-choline (Fig. 1). *L.*
334 *major* CPCT-null mutants (*cpct*⁻) cannot incorporate choline into PC but contain similar levels
335 of PC as WT parasites [45]. Loss of CPCT has no impact on promastigote growth in culture or
336 their virulence in mice [45]. A similar study on CEPT which is directly responsible for the
337 generation of diacyl-PE and PC revealed that this enzyme is only required for the promastigote
338 but not amastigote stage [18]. These findings indicate that intracellular amastigotes can survive
339 and proliferate without *de novo* PC synthesis by relying on the uptake/remodeling of host lipids.

340 Like with CEPT, chromosomal null mutants for *EPCT* cannot lose the complementing
341 pXNG4-EPCT episome in culture, suggesting that *de novo* PE synthesis is required for the fast-
342 replicating promastigotes (Fig. 4). The fact that EPCT is indispensable for amastigotes is
343 intriguing, as amastigotes can acquire enough PC, which is far more abundant than PE [18]. One
344 possibility is that the PE scavenging pathway, either direct uptake or remodeling of host lipids, is
345 insufficient and amastigotes need certain level of *de novo* synthesis to meet the demand for PE.
346 Alternatively, because of its central position in the Kennedy pathway, a loss of EPCT will not
347 only abolish the *de novo* synthesis of PME and diacyl-PE, but also negatively affect the
348 production of PC (from PE N-methylation) and PS (from PE interconversion). In comparison to

349 EPT, CPCT and CEPT, disruption of EPCT would result in a more pleiotropic effect on the
350 synthesis of multiple classes of glycerophospholipids (Fig. 1).

351 We observed a significant virulence attenuation from EPCT overexpression as parasites
352 with pXNG4-ECPT or pGEM-EPCT showed delayed lesion progression and cell replication in
353 mice (Fig. 5 and Fig. S7). Such defects were not found with the episomal overexpression EPT,
354 CPCT, CEPT, or FPPS (an essential enzyme required for sterol synthesis) [14, 18, 44, 45]. As a
355 cytosolic protein, EPCT generates CDP-EtN which is a substrate for EPT and CEPT to
356 synthesize PME and diacyl-PE, respectively (Fig. 1 and 2). Both EPT and CEPT are localized in
357 the endoplasmic reticulum (ER) [14, 18]. EPCT overexpression leads to reduced levels of PME
358 but has little effect on diacyl-PE or PC (Fig. 7 and 8), suggesting that increased production of
359 CDP-EtN is insufficient to boost PE synthesis and may instead cause substrate inhibition when
360 substrate concentrations exceed the optimum level for certain enzymes which hinders product
361 release [46]. It is not clear whether the altered PME synthesis in EPCT overexpressing cells is
362 responsible for their heightened sensitivity to starvation or acidic pH. Our previous report on *L.*
363 *major ept⁻* mutants indicate that while these mutants are largely devoid of PME, they did not
364 exhibit the same stress response defects as EPCT overexpressing cells [14]. It is possible that the
365 increased cytosolic concentration of CDP-EtN, coupled with the depletion of EtN-P, causes
366 cytotoxicity when parasite encounter starvation or acidic stress. We did not detect significant
367 changes in mitochondrial superoxide production from EPCT under- or over-expression,
368 suggesting that mitochondrial PE synthesis is not affected (Fig. S9).

369 While the alteration of *EPCT* expression had little impact on the cellular level of
370 lipophosphoglycan (LPG), it did significantly reduce the expression of GP63, a zinc-dependent
371 metalloprotease that plays pivotal role *Leishmania* infection through proteolytic cleavage of host

372 complement proteins and subversion of macrophage signaling [47-50]. As illustrated in Fig. 10,
373 *EPCT*^{+/-} parasites contained 20-25% of WT-level GP63; episomal expression of *EPCT* did not
374 rescue this defect and *epct*⁻+ pXNG4-*EPCT* cells had only 8-10% of WT-level GP63. These
375 results suggest that *EPCT* must be expressed from its endogenous locus to fully support GP63
376 synthesis, during which PE is used as a donor to generate the EtN-P linkage between protein and
377 GPI-anchor [7, 51].

378 In summary, our study establishes *EPCT* as the most important enzyme in the Kennedy
379 pathway. It is crucial for *L. major* survival during the promastigote and amastigote stages.
380 Overexpression of *EPCT* alters lipid homeostasis and stress response, leading to severely
381 attenuated virulence. Future studies will investigate how intracellular amastigotes balance *de*
382 *novo* synthesis with scavenging to optimize their long-term survival and evaluate the potential of
383 *EPCT* as a new anti-*Leishmania* target.

384 MATERIALS AND METHODS

385 Materials

386 Lipid standards for mass spectrometry studies including 1,2-dimyristoyl-sn-glycero-3-
387 phosphoethanolamine (14:0/14:0-PE), 1,2-dimyristoyl-sn-glycero-3-phosphocholine (14:0/14:0-
388 PC), and 1,2-dipalmitoyl-sn-glycero-3-phosphoinositol (16:0/16:0-PI) were purchased from
389 Avanti Polar Lipids (Alabaster, AL). For the EPCT activity assay, phosphoryl ethanolamine [1,2-
390 ^{14}C] (50-60 mCi/mmol) or [$^{14}\text{-C}$] EtN-P was purchased from American Radiolabeled Chemicals
391 (St Louis, MO). All other reagents were purchased from Thermo Fisher Scientific or Sigma
392 Aldrich Inc unless otherwise specified.

393 *Leishmania* culture and genetic manipulations

394 *Leishmania major* strain FV1 (MHOM/IL/81/Friedlin) promastigotes were cultivated at
395 27 °C in a complete M199 medium (M199 with 10% heat inactivated fetal bovine serum and
396 other supplements, pH 7.4) [52]. To monitor growth, culture densities were measured daily by
397 hemocytometer counting. Log phase promastigotes refer to replicative parasites at densities <1.0
398 $\times 10^7$ cells/ml, and stationary phase promastigotes refer to non-replicative parasites $>2.0 \times 10^7$
399 cells/ml.

400 To delete chromosomal *EPCT* alleles, the upstream and downstream flanking sequences
401 (~1 Kb each) of *EPCT* were amplified by PCR and cloned in the pUC18 vector. Genes
402 conferring resistance to blasticidin (*BSD*) and puromycin (*PAC*) were then cloned between the
403 upstream and downstream flanking sequences to generate pUC18-KO-EPCT:BSD and pUC18-
404 KO-EPCT:PAC, respectively. To generate the *EPCT* \pm heterozygotes ($\Delta EPCT::BSD/EPCT$),
405 wild type (WT) *L. major* promastigotes were transfected with linearized *BSD* knockout fragment
406 (derived from pUC18-KO-EPCT:BSD) by electroporation and transfectants showing resistance

407 to blasticidin were selected and later confirmed to be *EPCT*^{+/-} by Southern blot as previously
408 described [18]. To delete the second chromosomal allele of *EPCT*, we used an episome assisted
409 approach as previously described [42]. First, the *EPCT* open reading frame (ORF) was cloned
410 into the pXNG4 vector to generate pXNG4-*EPCT* and the resulting plasmid was introduced into
411 *EPCT*^{+/-} parasites. The resulting *EPCT*^{+/-} +pXNG4-*EPCT* cell lines were then transfected with
412 linearized *PAC* knockout fragment (derived from pUC18-KO-*EPCT*:BSD) and selected with 15
413 µg/ml of blasticidin, 15 µg/ml of puromycin and 150 µg/ml of nourseothricin. The resulting
414 *EPCT* chromosomal null mutants with pXNG4-*EPCT* ($\Delta EPCT::BSD/\Delta EPCT::PAC$ + pXNG4-
415 *EPCT* or *epct*⁻ + pXNG4-*EPCT*) were validated by Southern blot as described in Fig. 2, Fig. S2
416 and S3. For *EPCT* activity assay and localization studies, the *EPCT* ORF was into the pXG
417 vector or pXG-GFP' vector to generate pXG-*EPCT* or pXG-GFP-*EPCT* respectively, followed
418 by their introduction into WT *L. major* promastigotes by electroporation. Finally, a pGEM-5'-
419 Phleo-DST IR-*EPCT*-3' construct was generated by cloning the *EPCT* ORF along with its
420 upstream- and downstream flanking sequences (~1 Kb each) into a pGEM vector [53]. The
421 resulting plasmid was introduced into *EPCT*^{+/-} to drive *EPCT* overexpression in the presence of
422 its flanking sequences.

423 **EPCT activity assay**

424 EPCT assay was adopted based on a previously protocol [35]. Log phase promastigotes
425 of WT, WT + pXG-*EPCT*, and WT + pXG-GFP-*EPCT* were resuspended in a lysis buffer based
426 phosphate-buffered saline (PBS, pH 7.4) with 5 mM MgCl₂, 0.1% Triton X-100, 5 mM DTT,
427 and 1 X protease inhibitor cocktail at 4 x 10⁸ cells/ml. *Leishmania* lysate was incubated with 1
428 µCi of [¹⁴-C] EtN-P in a reaction buffer (100 mM Tris pH 7.5, 10 mM MgCl₂, and 5 mM CTP) at
429 room temperature for 20 min, boiled at 100 °C for 5 min to stop the reaction, and loaded directly

430 on a Silica gel 60 TLC plate (10 μ l each). TLC was developed in 100% ethanol:0.5% NaCl:25%
431 ammonium hydroxide (10:10:1, v/v) and signals were detected via autoradiography at -80 °C.
432 Mouse liver homogenate (with similar protein concentration as *Leishmania* lysate) was used as a
433 positive control whereas boiled *Leishmania* lysate and mouse liver homogenate were included as
434 negative controls. To determine the mobility of EPCT substrate (EtN-P) and product (CDP-EtN),
435 non-radiolabeled EtN-P and CDP-EtN (40 nmol each) were loaded onto a Silica gel 60 TLC
436 plate and processed with the same solvent as described above, followed by 0.2% ninhydrin
437 spray.

438 **Fluorescence microscopy and western blot**

439 An Olympus BX51 Upright Epifluorescence Microscope equipped with a digital camera
440 was used to visualize the localization of GFP-EPCT and GP63 as previously described [14]. For
441 GFP-EPCT, WT + pXG-GFP-EPCT promastigotes were attached to poly-L-lysine coated
442 coverslips and fixed with 3.7% paraformaldehyde prior to visualization. GP63 staining of
443 unpermeabilized parasites was performed using an anti-GP63 monoclonal antibody (#96/126,
444 1:500, Abcam Inc.) at ambient temperature for 30 min, followed by washing and incubation with
445 a goat-anti-mouse-IgG-Texas Red antibody (1:500) for 30 min.

446 To determine the cellular level of lipophosphoglycan (LPG), promastigote lysates were
447 boiled in SDS sample buffer at 95 °C for 5 min and resolved by SDS-PAGE. After transfer to
448 PVDF membrane, blots were probed with mouse anti-LPG monoclonal antibody WIC79.3
449 (1:1000) [54] followed by goat anti-mouse IgG conjugated with HRP (1:2000). GFP-EPCT and
450 GFP-C14DM were detected using a rabbit anti-GFP antibody (1:2000) followed by goat anti-
451 rabbit IgG-HRP (1:2000). Antibody to alpha-tubulin was used as the loading control.

452 **Promastigote essentiality assay**

453 WT, *EPCT*^{+/-} +pXNG4-EPCT, and *epct*⁻ + pXNG4-EPCT promastigotes were
454 inoculated in complete M199 media at 1.0×10^5 cells/ml in the presence or absence of 50 µg/ml
455 of GCV (the negative selection agent) or 150 µg/ml of nourseothricin (the positive selection
456 agent). Every three days, cells were reinoculated into fresh media with the same negative or
457 positive selection agents and percentages of GFP-high cells for each passage were determined by
458 flow cytometry using an Attune NxT Acoustic Flow Cytometer. After 14 passages, individual
459 clones of *EPCT*^{+/-} +pXNG4-EPCT and *epct*⁻ + pXNG4-EPCT were isolated via serial dilution
460 in 96-well plates. The GFP-high levels and pXNG4-EPCT plasmid copy numbers of selected
461 clones were determined by flow cytometry and qPCR, respectively.

462 **Mouse footpad infection and *in vivo* GCV treatment**

463 Female BALB/c mice (7-8 weeks old) were purchased from Charles River Laboratories
464 International (Wilmington, MA). All animal procedures were performed as per approved
465 protocol by Animal Care and Use Committee at Texas Tech University (PHS Approved Animal
466 Welfare Assurance No A3629-01). To determine whether EPCT is required during the
467 intracellular amastigote stage, day 3 stationary phase promastigotes were injected into the left
468 hind footpad of BALB/c mice (1.0×10^6 cells/mouse, 10 mice per group). For each group,
469 starting from day one post infection, one half of the mice received GCV at 7.5 mg/kg/day for 14
470 consecutive days (0.5 ml each, intraperitoneal injection), while the other half (control group)
471 received equivalent volume of sterile PBS. Footpad lesions were measured weekly using a
472 Vernier caliper after anesthetization with isoflurane (air flow rate: 0.3-0.5 ml/hour). Mice were
473 euthanized through controlled flow of CO₂ asphyxiation when lesions reached 2.5 mm (humane
474 endpoint) or upon the onset of secondary infections. Parasite numbers in infected footpads were
475 determined by limiting dilution assay [55] and qPCR as described below.

476 **Quantitative PCR (qPCR) analysis**

477 To determine parasite loads in infected footpads, genomic DNA was extracted from
478 footpad homogenate and qPCR reactions were run in triplicates using primers targeting the 28S
479 rRNA gene of *L. major* [18]. Cycle threshold (Ct) values were determined from melt curve
480 analysis. A standard curve of Ct values was generated using serially diluted genomic DNA
481 samples from *L. major* promastigotes (from 0.1 cell/reaction to 10⁵ cells/reaction) and Ct
482 values >30 were considered negative. Parasite numbers in footpad samples were calculated from
483 their Ct values using the standard curve. Control reactions included sterile water and DNA
484 extracted from uninfected mouse liver.

485 To determine pXNG4-*EPCT* plasmid levels in promastigotes and lesion-derived
486 amastigotes, a similar standard curve was generated using serially diluting pXNG4-EPCT
487 plasmid DNA (from 0.1 copy/reaction to 10⁵ copies/reaction) and primers targeting the *GFP*
488 region. qPCR was performed with the same set of primers on DNA samples and the average
489 plasmid copy number per cell was determined by dividing total plasmid copy number with total
490 parasite number based on Ct values.

491 To determine EPCT transcript levels, total RNA was extracted from promastigotes or
492 lesion-derived amastigotes and converted into cDNA using a high-capacity reverse transcription
493 kit (Bio-Rad), followed by qPCR using primers targeting *EPCT* or α -tubulin coding sequences.
494 The relative expression level of *EPCT* was normalized to that of α -tubulin using the $2^{-\Delta\Delta(Ct)}$
495 method [56]. Control reactions were carried out without leishmanial RNA and without reverse
496 transcriptase.

497 **Lipid extraction and mass spectrometric analyses**

498 Total lipids from stationary phase promastigotes (1.0×10^8 cells/sample) were extracted
499 using the Bligh & Dyer method [57]. Commercial non-indigenous lipid standards were added to
500 cell lysates as internal standards at the time of lipid extraction (1.0×10^8 molecules/cell for
501 14:0/14:0-PE, 5.0×10^7 molecules/cell for 14:0/14:0-PC, and 1.0×10^8 molecules/cell for
502 16:0/16:0-PI). These lipid standards are absent from *L. major* promastigotes. Determination of
503 lipid families by electrospray ionization mass spectrometry (ESI-MS) was carried out by a
504 Thermo Vantage TSQ instrument applying precursor ion scan of m/z 196 for PE, precursor ion
505 scan of m/z 241 for PI and IPC in the negative-ion mode, and precursor ion scan of m/z 184 for
506 PC in the positive-ion mode [58]. Individual lipid species and their structures were also
507 confirmed by high resolution mass spectrometry performed on a Thermo LTQ Orbitrap Velos
508 with a resolution of 100,000 (at m/z 400). All lipidomic analyses were performed five times.

509 ***Leishmania* stress response assays and determination of mitochondrial ROS level**

510 For heat tolerance, *L. major* promastigotes grown in complete M199 media were
511 incubated at either 27 °C or 37 °C. To test their sensitivity to acidic pH, promastigotes were
512 transferred to a pH5.0 medium (same as the complete M199 medium except that the pH was
513 adjusted to 5.0 using hydrochloric acid). For starvation response, promastigotes were transferred
514 to PBS (pH 7.4). Cell viability was determined at the indicated times by flow cytometry after
515 staining with 5 µg/ml of propidium iodide. Parasite growth was monitored by cell counting using
516 a hemocytometer.

517 Mitochondrial superoxide accumulation was determined as described previously [34].
518 Briefly, log phase promastigotes were transferred to PBS (pH 7.4) and stained with 5 µM of
519 MitoSox Red. After 25 min incubation at 27 °C, the mean fluorescence intensity (MFI) for each
520 sample was measured by flow cytometry.

521 **Statistical analysis**

522 Unless otherwise specified, experiments were repeated three to five times. Symbols or
523 bars represent averaged values and error bars represent standard deviations. Differences between
524 groups were assessed by one-way ANOVA (for three or more groups) using the Sigmaplot 13.0
525 software (Systat Software Inc, San Jose, CA) or student *t* test (for two groups). *P* values were
526 grouped in all figures (***: $p < 0.001$, **: $p < 0.01$, *: $p < 0.05$).

527 **ACKNOWLEDGMENTS**

528 This study was supported by NIH grants R15AI156746 (PI) and R01AI139198 (co-I) to
529 KZ. Lipidomic analysis was supported by NIH grants P41-GM103422, P60-DK20579, P30-
530 DK56341 to the Biomedical Mass Spectrometry Resource at Washington University in St. Louis.

531

532 **AUTHOR CONTRIBUTIONS**

533 Conceptualization and Project Design: Somrita Basu, Kai Zhang

534 Data Generation: Somrita Basu, Mattie Pawlowic, Fong-Fu Hsu, Geoff Thomas

535 Formal data analysis: Somrita Basu, Kai Zhang, Fong-Fu Hsu

536 Investigation: Somrita Basu, Kai Zhang, Fong-Fu Hsu

537 Fund Acquisition: Kai Zhang, Fong-Fu Hsu

538 Writing: Somrita Basu, Kai Zhang

539

540 **CONFLICT OF INTEREST**

541 The authors declare no competing interest

542

543 **FIGURE LEGENDS**

544 **Figure 1. Synthesis of PE and PC in *Leishmania*.** SPT: Serine palmitoyltransferase;
545 SK: Sphingosine kinase; SPL: sphingosine-1-phosphate lyase; EK: ethanolamine kinase; EPCT:
546 ethanolaminephosphate cytidyltransferase; EPT: ethanolamine phosphotransferase; CK: choline
547 kinase; CPCT: cholinephosphate cytidyltransferase; CEPT: choline ethanolamine
548 phosphotransferase; PEMT: Phosphatidylethanolamine N-methyltransferase; EtN: ethanolamine;
549 EtN-P: ethanolamine phosphate; AAG: 1-alkyl2-acyl glycerol; DAG: 1,2-diacylglycerol; CTP:
550 cytidine triphosphate; CDP: cytidine diphosphate; CMP: cytidine monophosphate; PPi:
551 pyrophosphate; PME: plasmenylethanolamine; diacyl PE: 1,2-diacyl-phosphatidylethanolamine,
552 PC: 1,2-diacyl-phosphatidylcholine; SAM: S-adenosyl-L-methionine; SAH: S-adenosyl-L-
553 homocysteine.

554 **Figure 2. *L. major* EPCT is a functional enzyme located in the cytoplasm.** (A) Whole cell
555 lysates (boiled and unboiled, two repeats each) of WT, WT+EPCT, and WT+GFP-EPCT
556 promastigotes were incubated with [¹⁴C]-EtN-P followed by TLC analysis as described in
557 *Materials and Methods*. (B) Promastigote lysates of WT, WT+GFP-EPCT, and WT+C14DM-
558 GFP (a control) were probed with an anti-GFP antibody (top) or anti- α -tubulin antibody
559 (bottom). (C) Log phase (top) and stationary phase(bottom) promastigotes of WT+GFP-EPCT
560 were examined by fluorescence microscopy. DIC: differential interference contrast. Scale bars:
561 10 μ m.

562 **Figure 3. Generation of chromosomal *EPCT*-null mutants using an episome-assisted**
563 **approach.** (A-D) Genomic DNA samples from FV1 WT, *EPCT*^{+/-} + pXNG4-*EPCT* (clone
564 #2B), and *epct*⁻ + pXNG4-*EPCT* (seven clones) parasites were digested with *Aat* II (A, B) or
565 *Kpn* I+*Avr* II (C, D) and analyzed by Southern blot using radiolabeled probes for an upstream

566 flanking sequence (**A, B**) or the open reading frame of *EPCT* (**C, D**). DNA loading controls with
567 ethidium bromide staining for **A** and **C** were included in **B** and **D**, respectively. The scheme of
568 Southern blot and expected DNA fragment sizes were shown in Fig. S3. (**E**) Promastigotes of
569 WT, *EPCT*^{+/-} (#2), WT + pXNG4-*EPCT*, *EPCT*^{+/-} + pXNG4-*EPCT* (clone #2B), and *epct*⁻
570 +pXNG4-*EPCT* (clone #2B-10) were cultivated at 27 °C in complete M199 media and culture
571 densities were determined daily using a hemocytometer. Error bars indicate standard deviations
572 from three biological repeats.

573 **Figure 4. EPCT is indispensable during the promastigote stage.** (**A**) Promastigotes were
574 continuously cultivated in the presence or absence of ganciclovir (GCV) or nourseothricin (SAT)
575 and passed every three days. Percentages of GFP-high cells were determined for every passage.
576 Error bars represent standard deviations from three repeats (**: $p < 0.01$, ***: $p < 0.001$). (**B-D**)
577 After 14 passages, WT (**B**) and *epct*⁻+pXNG4-*EPCT* parasites grown in the presence of SAT
578 (**C**) or GCV (**D**) were analyzed by flow cytometry to determine the percentages of GFP-high
579 cells (indicated by R2 in the histogram). (**E-F**) Two clones were isolated from the GFP-low
580 population in **D** by sorting, amplified in the absence of SAT, and analyzed for GFP expression
581 levels by flow cytometry.

582 **Figure 5. EPCT is indispensable during the amastigote stage.** BALB/c mice were infected in
583 the footpad with stationary phase promastigotes and treated with GCV or PBS as described in
584 *Materials and Methods*. (**A**) Sizes of footpad lesions for infected mice were measured weekly.
585 (**B**) Parasite numbers in infected footpads were determined by limiting dilution assay at the
586 indicated times. Data for WT and *EPCT*^{+/-} amastigotes were not available post 8 weeks when
587 those infected mice had reached the humane endpoint. (**C**) The pXNG4-*EPCT* plasmid copy

588 numbers in promastigotes and amastigotes (#/cell \pm SDs) were determined by qPCR. Error bars
589 represent standard deviations from three repeats (*: $p < 0.05$, **: $p < 0.01$, ***: $p < 0.001$).

590 **Figure 6. Expression level of *EPCT* mRNA in promastigotes and amastigotes.** Total RNA
591 was extracted from promastigotes (Pro) or amastigotes and the relative *EPCT* transcript levels
592 were determined by qRT-PCR using the $\Delta\Delta C_t$ method with α -tubulin gene being the internal
593 control. (A) WT promastigotes and WT amastigotes (6 weeks post infection). (B) Promastigotes
594 grown in the absence (WT and *EPCT*^{+/-}) or presence of SAT (WT+pXNG4-*EPCT*, *EPCT*^{+/-}
595 +pXNG4-*EPCT* and *epct*⁻+pXNG4-*EPCT*). (C) Lesion derived amastigotes from mice treated
596 with GCV or PBS (weeks 6 for WT and *EPCT*^{+/-}, week 14-20 for *EPCT* overexpressors). Error
597 bars represent standard deviation from three independent repeats (**: $p < 0.01$, ***: $p < 0.001$).

598 **Figure 7. *EPCT* overexpression leads to reduced levels of PME.** Total lipids were extracted
599 from promastigotes and analyzed by ESI-MS in the negative ion mode (see text in the “Materials
600 and Methods” for details). The 14:0/14:0-PE (m/z 634.5; [M – H]⁻ ion) was added as an internal
601 standard. (A) Representative chromatograms of precursor ion scan of m/z 196 specifically
602 monitoring PME and diacyl-PE species in a mixture. Common PME species such as *p*18:0/18:2-
603 PE (m/z: 726.5) and *p*18:0/18:1-PE (m/z: 728.5) were indicated. (B) Plot of abundance of PME
604 and diacyl PE lipids in different promastigote samples. Error bars represent standard deviation
605 from 5 independent experiments (*: $p < 0.05$, **: $p < 0.01$, ***: $p < 0.001$).

606 **Figure 8. *EPCT* overexpression does not affect the synthesis of PC.** Total lipids were
607 extracted from promastigotes and analyzed by ESI-MS in the positive ion mode (see text in the
608 “Materials and Methods” for details). The 14:0/14:0-PC (m/z 678.5; [M + H]⁺ ion) was added as
609 an internal standard. (A) Representative chromatograms of precursor ion scan of m/z 184
610 specifically monitoring PC and sphingomyelin species in a mixture. The structures of common

611 PC species were illustrated. **(B)** Plot of abundance of PC lipids in different promastigote
612 samples. Error bars represent standard deviation from 5 independent experiments.

613 **Figure 9. EPCT overexpression leads to reduced levels of PI.** Total lipids were extracted from
614 promastigotes and analyzed by ESI-MS in the negative ion mode. The 16:0/16:0-PI (m/z: 809.6)
615 was added as an internal standard. **(A)** Representative chromatograms of precursor ion scan for
616 m/z 241 (specific for PI). Common PI species were indicated. **(B)** Abundance of PI in
617 promastigotes. Error bars represent standard deviation from 4 independent experiments (**: $p <$
618 0.01, ***: $p < 0.001$).

619 **Figure 10. EPCT overexpression leads to reduced level of GP63 but not LPG.** **(A)** WT,
620 *EPCT*^{+/-}, WT + pXNG4-*EPCT*, *EPCT*^{+/-} + pXNG4-*EPCT*, and *epct*⁻ + pXNG4-*EPCT*
621 promastigotes were labeled with an anti-GP63 monoclonal antibody followed by an anti-mouse
622 IgG-Texas Red antibody (left: DIC, right: fluorescence). **(B)** Whole cell lysates from stationary
623 phase promastigotes were analyzed by western blot using an anti-*L. major* LPG antibody (top) or
624 anti- α -tubulin antibody (bottom). The relative abundances of GP63 **(C)** and LPG **(D)** were
625 determined and normalized to WT levels. Error bars represent standard deviations from 3
626 independent repeats (***: $p < 0.001$).

627 **Figure 11. EPCT overexpression leads to heightened sensitivity to acidic pH and starvation**
628 **conditions.** **(A-B)** Promastigotes were cultivated in regular M199 media (pH 7.4) at 27 °C until
629 reaching stationary phase. Cells were then kept in M199 media **(A)** or transferred into PBS **(B)**.
630 **(C-D)** Stationary phase **(C)** or log phase **(D)** promastigotes were cultivated in an acidic M199
631 medium (pH5.0). **(E-F)** Day 1 stationary phase promastigotes were inoculated in complete M199
632 media (pH 7.4) and incubated at 27 °C **(E)** or 37 °C **(F)**. Percentage of dead cells were measured
633 by flow cytometry after propidium iodide staining **(A-C, E and F)** and cell growth was

634 determined by hemocytometer counting (**D**). Error bars represent standard deviations from 3-4
635 independent experiments (*: $p < 0.05$, **: $p < 0.01$, ***: $p < 0.001$).

636 **SUPPORTING INFORMATION**

637 **Figure S1. Figure S1. Alignment of EPCT amino acid sequences from *Saccharomyces***
638 ***cerevisiae* (*Sc*, Genbank: P33412), *Plasmodium falciparum* (*Pf*, Plasmodb:**
639 **PfDd2_130053500), *Leishmania major* (*Lm*, Tritypdb: LmjF.32.0890), *Arabidopsis thaliana***
640 **(*At*, TAIR: AT2G38670.1), and *Homo sapiens* (*Hs*, Genbank: Q99447) using Clustal**
641 **Omega. Asterisks (*): fully conserved residues; colons (:): highly similar residues; periods (.):**
642 **moderately similar residues. Color code for amino acids: red-nonpolar; green-polar; blue-acidic;**
643 **purple-basic.**

644 **Figure S2. Detection of EPCT activity with thin layer chromatography (TLC). (A)** EtN-P or
645 CDP-EtN (40 nmol each) are resolved by TLC as described in *Materials and Methods*. The plate
646 was dried and sprayed with 0.2% ninhydrin to show the positions of EtN-P and CDP-EtN. **(B)**
647 Mouse liver lysates (boiled and un-boiled, two repeats each) were incubated with [¹⁴C]-EtN-P at
648 room temperature, followed by TLC analysis and signals were detected by autoradiography.

649 **Figure S3. Chromosomal EPCT-null mutants cannot be generated without a**
650 **complementing episome.** Genomic DNA samples from *L. major* FV1 WT, LV39 WT, *EPCT*^{+/-}
651 (#1 and #2), and putative *epct*⁻ (#1D, #1E, and #1F) parasites were digested by *Hind* III + *Bam*
652 HI followed by Southern blot analyses using radiolabeled probes for an upstream flanking
653 sequence (5' probe: **A** and **C**) and the open reading frame of *EPCT* (ORF probe: **B** and **D**). The
654 approximate recognition sites of *Hind* III and *Bam* HI and expected DNA fragment sizes are
655 indicated in **E**.

656 **Figure S4. The scheme of Southern blot in Fig. 2.** Expected DNA fragment sizes for using the
657 5' probe (**A-B**) or ORF probe of *EPCT* (**C-D**) are indicated. TK: thymidine kinase, GFP: green
658 fluorescent protein, SAT: nourseothricin resistance gene.

659 **Figure S5. Chromosomal *EPCT*-null promastigotes cannot lose the pXNG4-EPCT episome.**

660 (A) *EPCT*^{+/-} + pXNG4-EPCT and *epct*⁻ + pXNG4-EPCT promastigotes were cultivated in the
661 presence of SAT or GCV for 14 passages (as pools) and individual clones were isolated via
662 sorting followed by serial dilution. Plasmid copy number numbers (average ± SDs) were
663 determined by qPCR. (B) Promastigotes were cultivated at 27 °C in complete M199 media and
664 culture densities were determined daily using a hemocytometer. Error bars indicate standard
665 deviations from three biological repeats (**: $p < 0.01$).

666 **Figure S6. EPCT overexpression leads to reduced growth in BALB/c mice.** Following

667 footpad infection, mice were treated with GCV or PBS and euthanized at the indicated
668 timepoints. (A) Mouse body weights were measured at day 0-21 post infection. (B) Genomic
669 DNA samples were prepared from lesion-derived amastigotes and parasite loads were
670 determined by qPCR using primers targeting the *L. major* 28S rDNA gene (*: $p < 0.05$, **: $p <$
671 0.01 , ***: $p < 0.001$).

672 **Figure S7. EPCT overexpression leads to attenuated virulence in BALB/c mice.** Stationary

673 phase promastigotes were injected into the footpad of BALB/c mice as described in *Materials*
674 *and Methods*. Footpad lesion sizes were measured using a Vernier caliper (A) and parasite loads
675 were determined by qPCR (B). **: $p < 0.01$.

676 **Figure S8. EPCT overexpression does not affect the cellular levels of IPC.** Total lipids were

677 extracted from stationary phase promastigotes and analyzed by ESI/MS in the negative ion mode
678 using both total ion current scan and precursor ion scan of m/z 241. Error bars represent standard
679 deviations from 4 independent experiments.

680 **Figure S9. EPCT overexpression does not affect mitochondrial ROS production.** Log phase

681 promastigotes were cultivated in complete M199 medium (A, C) or transferred to PBS (B, D)

682 and labeled with MitoSox Red for 25 min. Mean fluorescence intensity (MFI) for MitoSox Red
683 **(A, B)** and percentages of dead cells **(C, D)** were determined by flow cytometry at the indicated
684 timepoints. Cell growth rates were determined by hemocytometer counting **(E)**. Error bars
685 represent standard deviations from three independent experiments.

686 **Table S1. List of oligonucleotides used in this study.** Sequences in lowercase represent
 687 restriction enzyme sites.

Primer	Name	Sequence
#52	5' UTR EPCT forward	CATGACgaattcGACCAGCAACGTGAGGGAC
#12	5' UTR EPCT reverse	TCAGACACTAGTGATCATGGATCCGGTGGCGGCAGAAGTGG AAG
#13	3' UTR EPCT forward	TCAGTAggatccCGTAGTGGGCTGGCGGGGAG
#14	3' UTR EPCT reverse	GATCATaagcttCAAATAAAGAGAGTCAGTG
#9	EPCT ORF forward	GATCAGggatccACCATGCCCACCGTTTCTTCG
#10	EPCT ORF reverse	GACTACggatccCTAGCTTGCCTCCCGTAATTTG
#73	EPCT 5' UTR Southern forward	AGCACTTGCTCCAAGCGAAGAG
#74	EPCT 5' UTR Southern reverse	GAACAAGAAGCCGTACTTCACAG
#15	EPCT ORF Southern forward	GCCGAGGAGCGCTATGAGGC
#16	EPCT ORF Southern reverse	GAGAACTTGTCGCCTACAAC
#699	28S rRNA qPCR forward	AAGATGGACCGGCCTCTAGT
#700	28S rRNA qPCR reverse	ATCCTTCCCCGCTCCAGTAT
#703	pXNG4 qPCR forward	CCCGACAACCACTACCTGAG
#704	pXNG4 qPCR reverse	GTCCATGCCGAGAGTGATCC
#842	EPCT ORF RT forward	CATGAGCTTCAACGAGCGTG
#843	EPCT ORF RT reverse	GCCGTCAATCACATCCTTGC

688

689

690 **REFERENCES**

- 691 1. Alvar J, Velez ID, Bern C, Herrero M, Desjeux P, Cano J, et al. Leishmaniasis worldwide
692 and global estimates of its incidence. *PloS one*. 2012;7(5):e35671. Epub 2012/06/14. doi:
693 10.1371/journal.pone.0035671. PubMed PMID: 22693548; PubMed Central PMCID:
694 PMC3365071.
- 695 2. DALYs GBD, Collaborators H, Murray CJ, Barber RM, Foreman KJ, Abbasoglu
696 Ozgoren A, et al. Global, regional, and national disability-adjusted life years (DALYs) for 306
697 diseases and injuries and healthy life expectancy (HALE) for 188 countries, 1990-2013:
698 quantifying the epidemiological transition. *Lancet*. 2015;386(10009):2145-91. Epub 20150828.
699 doi: 10.1016/S0140-6736(15)61340-X. PubMed PMID: 26321261; PubMed Central PMCID:
700 PMCPMC4673910.
- 701 3. Croft SL, Sundar S, Fairlamb AH. Drug resistance in leishmaniasis. *Clinical*
702 *microbiology reviews*. 2006;19(1):111-26. PubMed PMID: 16418526.
- 703 4. Uliana SRB, Trinconi CT, Coelho AC. Chemotherapy of leishmaniasis: present
704 challenges. *Parasitology*. 2018;145(4):464-80. Epub 20170120. doi:
705 10.1017/S0031182016002523. PubMed PMID: 28103966.
- 706 5. Exton JH. Phosphatidylcholine breakdown and signal transduction. *Biochimica et*
707 *biophysica acta*. 1994;1212(1):26-42. Epub 1994/04/14. PubMed PMID: 8155724.
- 708 6. Furse S, de Kroon AI. Phosphatidylcholine's functions beyond that of a membrane brick.
709 *Mol Membr Biol*. 2015;32(4):117-9. Epub 20150825. doi: 10.3109/09687688.2015.1066894.
710 PubMed PMID: 26306852.

- 711 7. Menon AK, Eppinger M, Mayor S, Schwarz RT. Phosphatidylethanolamine is the donor
712 of the terminal phosphoethanolamine group in trypanosome glycosylphosphatidylinositols.
713 EMBO J. 1993;12(5):1907-14. PubMed PMID: 8491183.
- 714 8. Besteiro S, Williams RA, Morrison LS, Coombs GH, Mottram JC. Endosome sorting and
715 autophagy are essential for differentiation and virulence of *Leishmania major*. The Journal of
716 biological chemistry. 2006;281(16):11384-96. PubMed PMID: 16497676.
- 717 9. Williams RA, Smith TK, Cull B, Mottram JC, Coombs GH. ATG5 is essential for ATG8-
718 dependent autophagy and mitochondrial homeostasis in *Leishmania major*. PLoS pathogens.
719 2012;8(5):e1002695. Epub 2012/05/23. doi: 10.1371/journal.ppat.1002695. PubMed PMID:
720 22615560; PubMed Central PMCID: PMC3355087.
- 721 10. Signorell A, Jelk J, Rauch M, Butikofer P. Phosphatidylethanolamine is the precursor of
722 the ethanolamine phosphoglycerol moiety bound to eukaryotic elongation factor 1A. The Journal
723 of biological chemistry. 2008;283(29):20320-9. PubMed PMID: 18499667.
- 724 11. Kennedy EP. The synthesis of cytidine diphosphate choline, cytidine diphosphate
725 ethanolamine, and related compounds. The Journal of biological chemistry. 1956;222(1):185-91.
726 PubMed PMID: 13366992.
- 727 12. Zhang K, Pompey JM, Hsu FF, Key P, Bandhuvula P, Saba JD, et al. Redirection of
728 sphingolipid metabolism toward *de novo* synthesis of ethanolamine in *Leishmania*. EMBO J.
729 2007;26(4):1094-104. PubMed PMID: 17290222.
- 730 13. Sundler R. Ethanolaminephosphate cytidylyltransferase. Purification and characterization
731 of the enzyme from rat liver. The Journal of biological chemistry. 1975;250(22):8585-90.
732 PubMed PMID: 241749.

- 733 14. Pawlowic MC, Hsu FF, Moitra S, Biyani N, Zhang K. Plasmenylethanolamine synthesis
734 in *Leishmania major*. *Molecular microbiology*. 2016;101(2):238-49. Epub 2016/04/12. doi:
735 10.1111/mmi.13387. PubMed PMID: 27062077; PubMed Central PMCID: PMC4935589.
- 736 15. Ford DA. Separate myocardial ethanolamine phosphotransferase activities responsible for
737 plasmenylethanolamine and phosphatidylethanolamine synthesis. *Journal of lipid research*.
738 2003;44(3):554-9. Epub 2003/02/04. doi: 10.1194/jlr.M200426-JLR200. PubMed PMID:
739 12562835.
- 740 16. Signorell A, Rauch M, Jelk J, Ferguson MA, Butikofer P. Phosphatidylethanolamine in
741 *Trypanosoma brucei* is organized in two separate pools and is synthesized exclusively by the
742 Kennedy pathway. *The Journal of biological chemistry*. 2008;283(35):23636-44. PubMed PMID:
743 18587155.
- 744 17. Henneberry AL, McMaster CR. Cloning and expression of a human
745 choline/ethanolaminephosphotransferase: synthesis of phosphatidylcholine and
746 phosphatidylethanolamine. *The Biochemical journal*. 1999;339 (Pt 2):291-8. Epub 1999/04/07.
747 PubMed PMID: 10191259; PubMed Central PMCID: PMC1220157.
- 748 18. Moitra S, Basu S, Pawlowic M, Hsu FF, Zhang K. De Novo Synthesis of
749 Phosphatidylcholine Is Essential for the Promastigote But Not Amastigote Stage in *Leishmania*
750 *major*. *Frontiers in cellular and infection microbiology*. 2021;11:647870. Epub 20210312. doi:
751 10.3389/fcimb.2021.647870. PubMed PMID: 33777852; PubMed Central PMCID:
752 PMCPMC7996062.
- 753 19. Vance JE. Phosphatidylserine and phosphatidylethanolamine in mammalian cells: two
754 metabolically related aminophospholipids. *Journal of lipid research*. 2008;49(7):1377-87.
755 PubMed PMID: 18204094.

- 756 20. Vance DE. Phospholipid methylation in mammals: from biochemistry to physiological
757 function. *Biochimica et biophysica acta*. 2014;1838(6):1477-87. Epub 20131101. doi:
758 10.1016/j.bbamem.2013.10.018. PubMed PMID: 24184426.
- 759 21. Bibis SS, Dahlstrom K, Zhu T, Zufferey R. Characterization of *Leishmania major*
760 phosphatidylethanolamine methyltransferases LmjPEM1 and LmjPEM2 and their inhibition by
761 choline analogs. *Molecular and biochemical parasitology*. 2014;196(2):90-9. Epub 2014/09/02.
762 doi: 10.1016/j.molbiopara.2014.08.005. PubMed PMID: 25176160; PubMed Central PMCID:
763 PMC4252796.
- 764 22. Parodi-Talice A, Araujo JM, Torres C, Perez-Victoria JM, Gamarro F, Castanys S. The
765 overexpression of a new ABC transporter in *Leishmania* is related to phospholipid trafficking
766 and reduced infectivity. *Biochimica et biophysica acta*. 2003;1612(2):195-207. doi:
767 10.1016/s0005-2736(03)00131-7. PubMed PMID: 12787938.
- 768 23. Castanys-Munoz E, Alder-Baerens N, Pomorski T, Gamarro F, Castanys S. A novel
769 ATP-binding cassette transporter from *Leishmania* is involved in transport of
770 phosphatidylcholine analogues and resistance to alkyl-phospholipids. *Molecular microbiology*.
771 2007;64(5):1141-53. PubMed PMID: 17542911.
- 772 24. Zhang K. Balancing de novo synthesis and salvage of lipids by *Leishmania amastigotes*.
773 *Current opinion in microbiology*. 2021;63:98-103. Epub 20210723. doi:
774 10.1016/j.mib.2021.07.004. PubMed PMID: 34311265; PubMed Central PMCID:
775 PMC8463422.
- 776 25. Zhang K, Beverley SM. Phospholipid and sphingolipid metabolism in *Leishmania*.
777 *Molecular and biochemical parasitology*. 2010;170(2):55-64. PMCID: 2815228. PubMed PMID:
778 20026359.

- 779 26. Zhang K, Hsu FF. Shotgun Lipidomic Analysis of Leishmania Cells. *Methods Mol Biol.*
780 2021;2306:215-25. doi: 10.1007/978-1-0716-1410-5_14. PubMed PMID: 33954949.
- 781 27. Gossage SM, Rogers ME, Bates PA. Two separate growth phases during the
782 development of Leishmania in sand flies: implications for understanding the life cycle.
783 *International journal for parasitology.* 2003;33(10):1027-34. PubMed PMID: 13129524.
- 784 28. Inbar E, Akopyants NS, Charmoy M, Romano A, Lawyer P, Elnaiem DE, et al. The
785 mating competence of geographically diverse Leishmania major strains in their natural and
786 unnatural sand fly vectors. *PLoS genetics.* 2013;9(7):e1003672. Epub 2013/08/13. doi:
787 10.1371/journal.pgen.1003672. PubMed PMID: 23935521; PubMed Central PMCID:
788 PMC3723561.
- 789 29. Saunders EC, Ng WW, Kloehn J, Chambers JM, Ng M, McConville MJ. Induction of a
790 stringent metabolic response in intracellular stages of Leishmania mexicana leads to increased
791 dependence on mitochondrial metabolism. *PLoS pathogens.* 2014;10(1):e1003888. Epub
792 2014/01/28. doi: 10.1371/journal.ppat.1003888. PubMed PMID: 24465208; PubMed Central
793 PMCID: PMC3900632.
- 794 30. Mandell MA, Beverley SM. Continual renewal and replication of persistent Leishmania
795 major parasites in concomitantly immune hosts. *Proceedings of the National Academy of*
796 *Sciences of the United States of America.* 2017;114(5):E801-E10. Epub 2017/01/18. doi:
797 10.1073/pnas.1619265114. PubMed PMID: 28096392; PubMed Central PMCID: PMC5293024.
- 798 31. Kuhlmann FM, Key PN, Hickerson SM, Turk J, Hsu FF, Beverley SM. Inositol
799 phosphorylceramide synthase null Leishmania are viable and virulent in animal infections where
800 salvage of host sphingomyelin predominates. *The Journal of biological chemistry.*

801 2022;298(11):102522. Epub 20220923. doi: 10.1016/j.jbc.2022.102522. PubMed PMID:
802 36162499; PubMed Central PMCID: PMCPMC9637897.

803 32. Zhang K, Hsu FF, Scott DA, Docampo R, Turk J, Beverley SM. *Leishmania* salvage and
804 remodelling of host sphingolipids in amastigote survival and acidocalcisome biogenesis.
805 Molecular microbiology. 2005;55(5):1566-78. PubMed PMID: 15720561.

806 33. Xu W, Hsu FF, Baykal E, Huang J, Zhang K. Sterol Biosynthesis Is Required for Heat
807 Resistance but Not Extracellular Survival in *Leishmania*. PLoS pathogens.
808 2014;10(10):e1004427. Epub 2014/10/24. doi: 10.1371/journal.ppat.1004427. PubMed PMID:
809 25340392.

810 34. Mukherjee S, Moitra S, Xu W, Hernandez V, Zhang K. Sterol 14-alpha-demethylase is
811 vital for mitochondrial functions and stress tolerance in *Leishmania major*. PLoS pathogens.
812 2020;16(8):e1008810. Epub 20200820. doi: 10.1371/journal.ppat.1008810. PubMed PMID:
813 32817704; PubMed Central PMCID: PMCPMC7462297.

814 35. Tijburg LB, Vermeulen PS, van Golde LM. Ethanolamine-phosphate
815 cytidyltransferase. Methods Enzymol. 1992;209:258-63. PubMed PMID: 1323040.

816 36. Pavlovic Z, Bakovic M. Regulation of Phosphatidylethanolamine
817 Homeostasis—The Critical Role of CTP:Phosphoethanolamine Cytidyltransferase
818 (Pcyt2). Int J Mol Sci. 2013;14(2):2529-50. Epub 20130125. doi: 10.3390/ijms14022529.
819 PubMed PMID: 23354482; PubMed Central PMCID: PMCPMC3588000.

820 37. Fullerton MD, Hakimuddin F, Bakovic M. Developmental and metabolic effects of
821 disruption of the mouse CTP:phosphoethanolamine cytidyltransferase gene (Pcyt2). Mol Cell
822 Biol. 2007;27(9):3327-36. Epub 20070226. doi: 10.1128/MCB.01527-06. PubMed PMID:
823 17325045; PubMed Central PMCID: PMCPMC1899976.

- 824 38. Fullerton MD, Hakimuddin F, Bonen A, Bakovic M. The development of a metabolic
825 disease phenotype in CTP:phosphoethanolamine cytidylyltransferase-deficient mice. *The Journal*
826 *of biological chemistry*. 2009;284(38):25704-13. Epub 20090722. doi:
827 10.1074/jbc.M109.023846. PubMed PMID: 19625253; PubMed Central PMCID:
828 PMCPMC2757972.
- 829 39. Leonardi R, Frank MW, Jackson PD, Rock CO, Jackowski S. Elimination of the CDP-
830 ethanolamine pathway disrupts hepatic lipid homeostasis. *The Journal of biological chemistry*.
831 2009;284(40):27077-89. Epub 20090807. doi: 10.1074/jbc.M109.031336. PubMed PMID:
832 19666474; PubMed Central PMCID: PMCPMC2785637.
- 833 40. Ha DS, Schwarz JK, Turco SJ, Beverley SM. Use of the green fluorescent protein as a
834 marker in transfected *Leishmania*. *Molecular and biochemical parasitology*. 1996;77(1):57-64.
835 PubMed PMID: 8784772.
- 836 41. Beverley SM. Protozoomics: trypanosomatid parasite genetics comes of age. *Nat Rev*
837 *Genet*. 2003;4(1):11-9. PubMed PMID: 12509749.
- 838 42. Murta SM, Vickers TJ, Scott DA, Beverley SM. Methylene tetrahydrofolate
839 dehydrogenase/cyclohydrolase and the synthesis of 10-CHO-THF are essential in *Leishmania*
840 major. *Molecular microbiology*. 2009;71(6):1386-401. PubMed PMID: 19183277.
- 841 43. McCall LI, El Aroussi A, Choi JY, Vieira DF, De Muylder G, Johnston JB, et al.
842 Targeting Ergosterol biosynthesis in *Leishmania donovani*: essentiality of sterol 14 alpha-
843 demethylase. *PLoS neglected tropical diseases*. 2015;9(3):e0003588. Epub 2015/03/15. doi:
844 10.1371/journal.pntd.0003588. PubMed PMID: 25768284; PubMed Central PMCID:
845 PMC4359151.

- 846 44. Mukherjee S, Basu S, Zhang K. Farnesyl pyrophosphate synthase is essential for the
847 promastigote and amastigote stages in *Leishmania major*. *Molecular and biochemical*
848 *parasitology*. 2019;230:8-15. Epub 2019/03/31. doi: 10.1016/j.molbiopara.2019.03.001. PubMed
849 PMID: 30926449; PubMed Central PMCID: PMC6529949.
- 850 45. Moitra S, Pawlowic MC, Hsu FF, Zhang K. Phosphatidylcholine synthesis through
851 cholinephosphate cytidylyltransferase is dispensable in *Leishmania major*. *Scientific reports*.
852 2019;9(1):7602. Epub 2019/05/22. doi: 10.1038/s41598-019-44086-6. PubMed PMID:
853 31110206; PubMed Central PMCID: PMC6527706.
- 854 46. Kokkonen P, Beier A, Mazurenko S, Damborsky J, Bednar D, Prokop Z. Substrate
855 inhibition by the blockage of product release and its control by tunnel engineering. *RSC Chem*
856 *Biol*. 2021;2(2):645-55. Epub 20210111. doi: 10.1039/d0cb00171f. PubMed PMID: 34458806;
857 PubMed Central PMCID: PMC6527706.
- 858 47. Isnard A, Shio MT, Olivier M. Impact of *Leishmania* metalloprotease GP63 on
859 macrophage signaling. *Frontiers in cellular and infection microbiology*. 2012;2:72. Epub
860 2012/08/25. doi: 10.3389/fcimb.2012.00072. PubMed PMID: 22919663; PubMed Central
861 PMCID: PMC3417651.
- 862 48. Guay-Vincent MM, Matte C, Berthiaume AM, Olivier M, Jaramillo M, Descoteaux A.
863 Revisiting *Leishmania* GP63 host cell targets reveals a limited spectrum of substrates. *PLoS*
864 *pathogens*. 2022;18(10):e1010640. Epub 20221003. doi: 10.1371/journal.ppat.1010640. PubMed
865 PMID: 36191034; PubMed Central PMCID: PMC6527706.
- 866 49. Casgrain PA, Martel C, McMaster WR, Mottram JC, Olivier M, Descoteaux A. Cysteine
867 Peptidase B Regulates *Leishmania mexicana* Virulence through the Modulation of GP63
868 Expression. *PLoS pathogens*. 2016;12(5):e1005658. Epub 20160518. doi:

- 869 10.1371/journal.ppat.1005658. PubMed PMID: 27191844; PubMed Central PMCID:
870 PMCPMC4871588.
- 871 50. Brittingham A, Morrison CJ, McMaster WR, McGwire BS, Chang KP, Mosser DM. Role
872 of the Leishmania surface protease gp63 in complement fixation, cell adhesion, and resistance to
873 complement-mediated lysis. *J Immunol.* 1995;155(6):3102-11.
- 874 51. Field MC, Medina-Acosta E, Cross GA. Inhibition of glycosylphosphatidylinositol
875 biosynthesis in *Leishmania mexicana* by mannosamine. *The Journal of biological chemistry.*
876 1993;268(13):9570-7. PubMed PMID: 8387500.
- 877 52. Kapler GM, Coburn CM, Beverley SM. Stable transfection of the human parasite
878 *Leishmania major* delineates a 30-kilobase region sufficient for extrachromosomal replication
879 and expression. *Mol Cell Biol.* 1990;10(3):1084-94. PubMed PMID: 2304458.
- 880 53. Madeira da Silva L, Owens KL, Murta SM, Beverley SM. Regulated expression of the
881 *Leishmania major* surface virulence factor lipophosphoglycan using conditionally destabilized
882 fusion proteins. *Proceedings of the National Academy of Sciences of the United States of*
883 *America.* 2009;106(18):7583-8. PubMed PMID: 19383793.
- 884 54. de Ibarra AA, Howard JG, Snary D. Monoclonal antibodies to *Leishmania tropica major*:
885 specificities and antigen location. *Parasitology.* 1982;85 (Pt 3):523-31. PubMed PMID: 6184664.
- 886 55. Titus RG, Marchand M, Boon T, Louis JA. A limiting dilution assay for quantifying
887 *Leishmania major* in tissues of infected mice. *Parasite Immunol.* 1985;7(5):545-55. PubMed
888 PMID: 3877902.
- 889 56. Livak KJ, Schmittgen TD. Analysis of relative gene expression data using real-time
890 quantitative PCR and the 2⁻($\Delta\Delta C(T)$) Method. *Methods.* 2001;25(4):402-8. PubMed
891 PMID: 11846609.

- 892 57. Bligh EG, Dyer WJ. A rapid method of total lipid extraction and purification. Canadian
893 journal of biochemistry and physiology. 1959;37(8):911-7. PubMed PMID: 13671378.
- 894 58. Hsu FF. Mass spectrometry-based shotgun lipidomics - a critical review from the
895 technical point of view. Analytical and bioanalytical chemistry. 2018;410(25):6387-409. Epub
896 2018/08/11. doi: 10.1007/s00216-018-1252-y. PubMed PMID: 30094786; PubMed Central
897 PMCID: PMC6195124.
- 898

Fig. 1

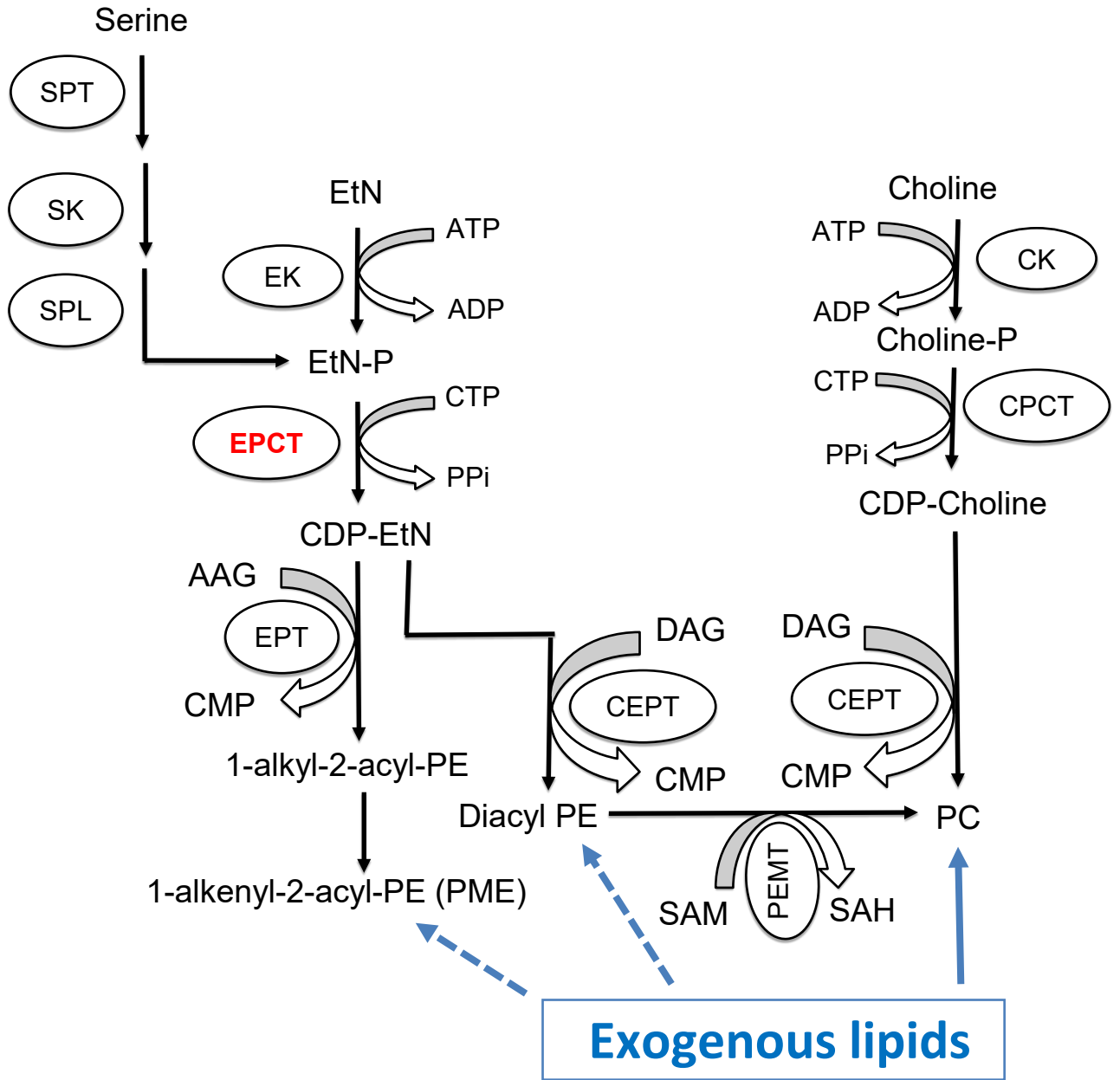


Fig. 2

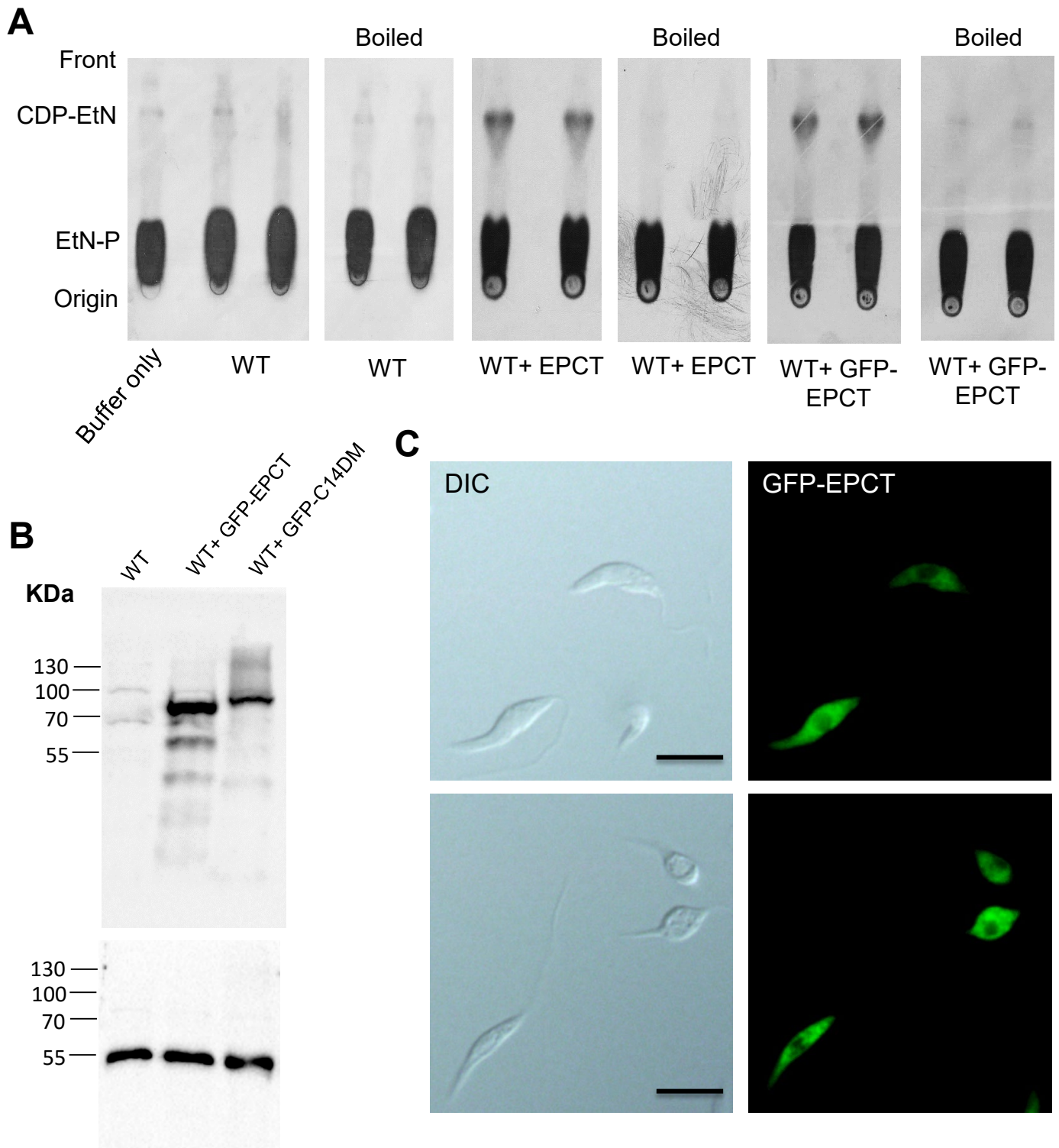


Fig. 3

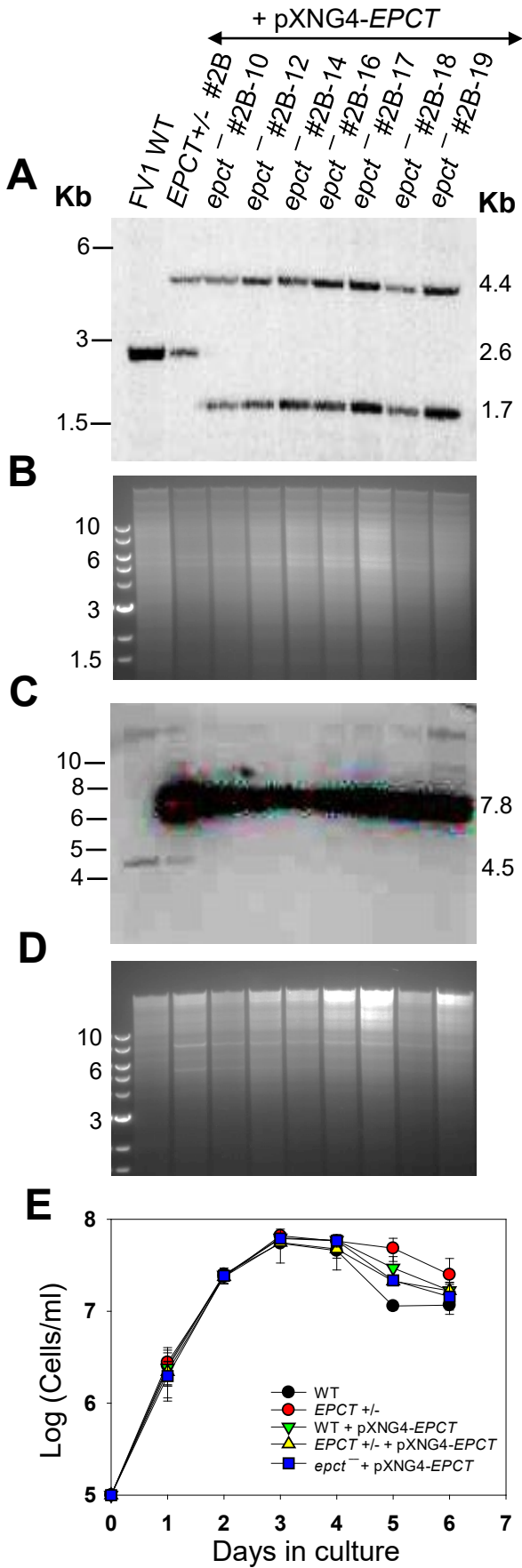
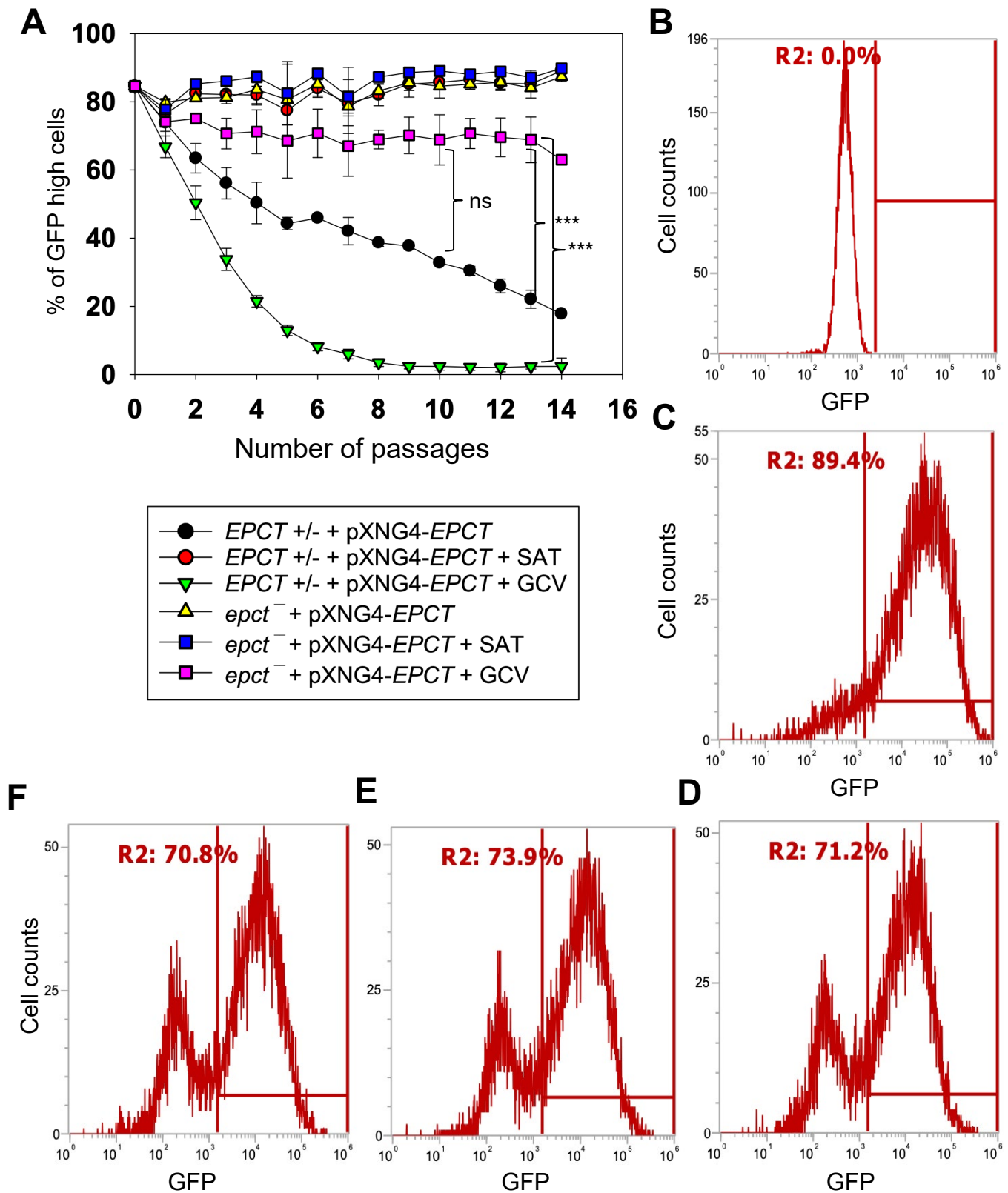


Fig. 4



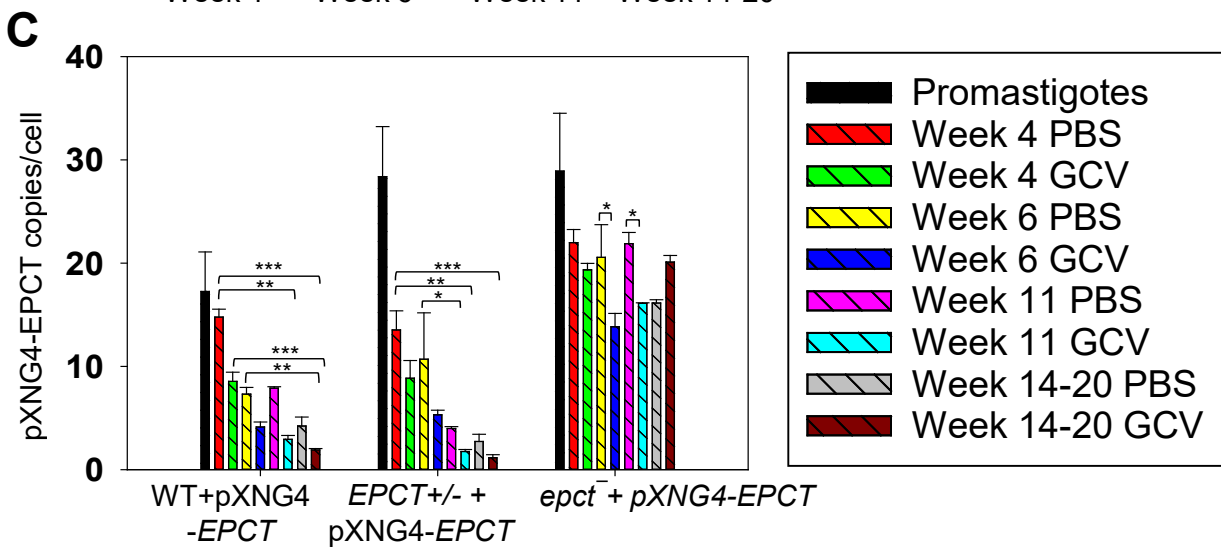
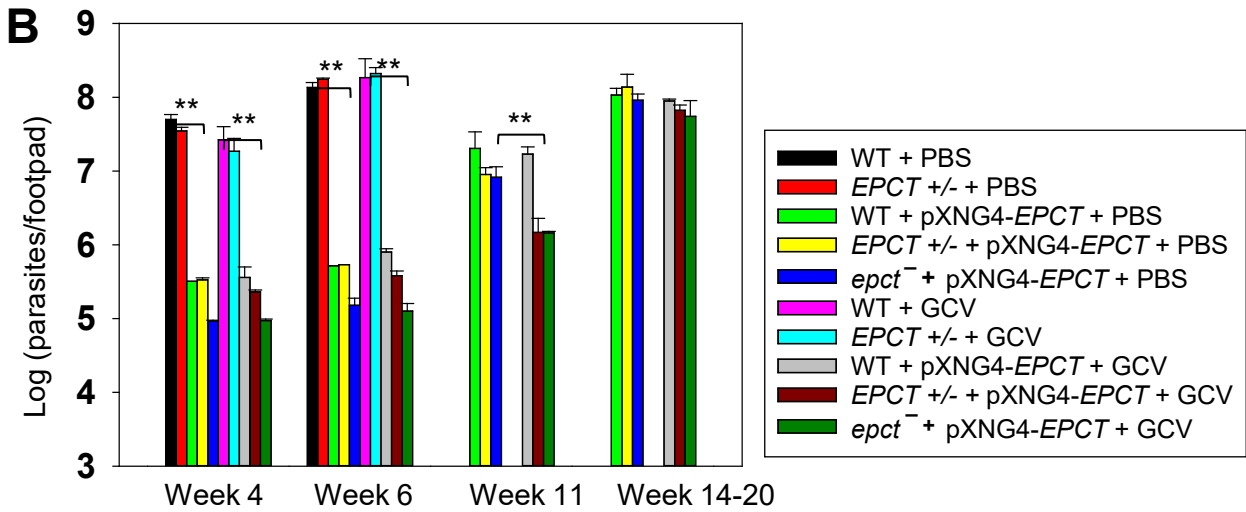
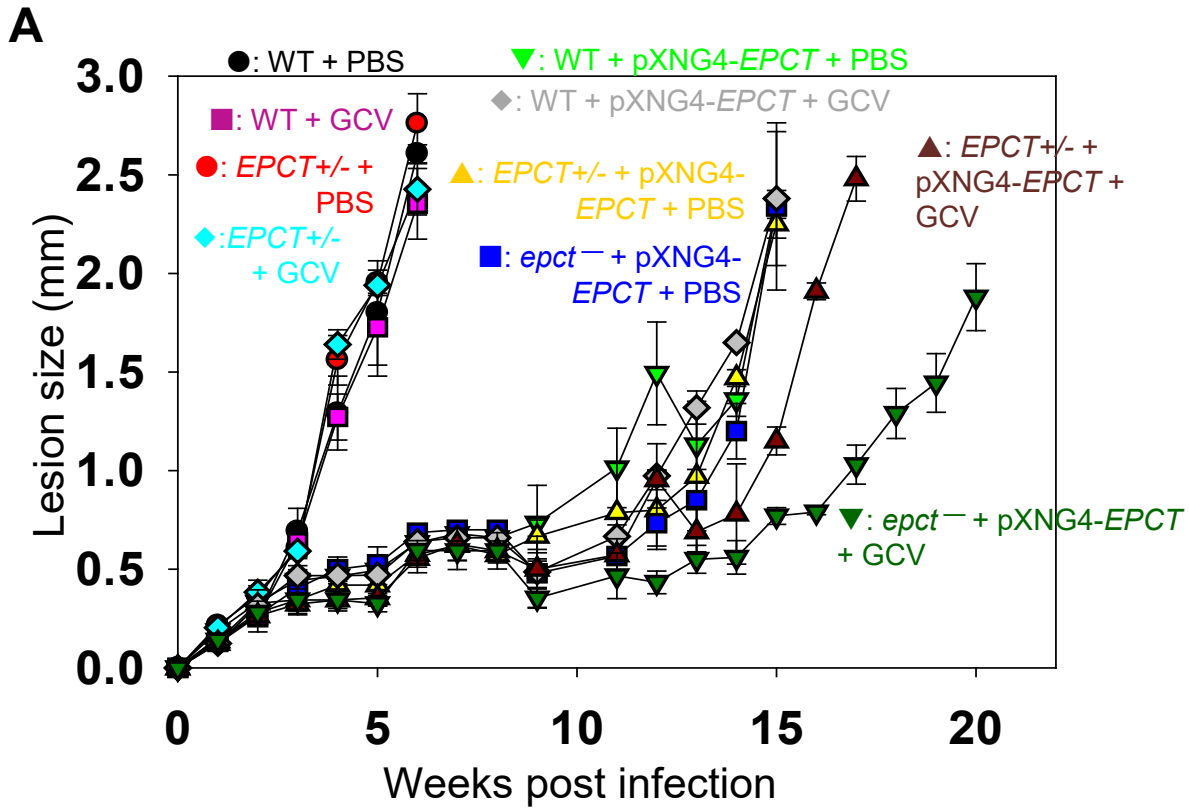


Fig. 6

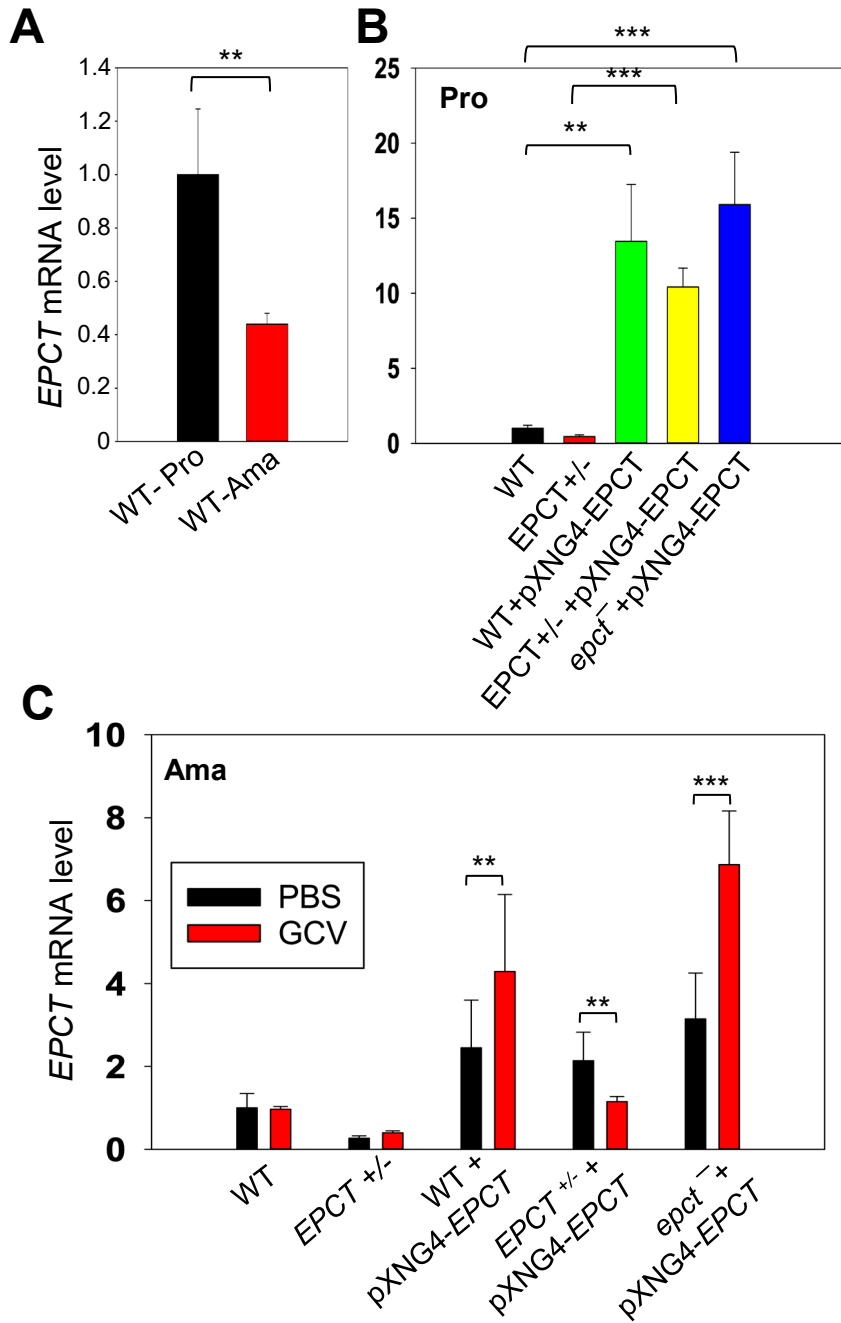


Fig. 7

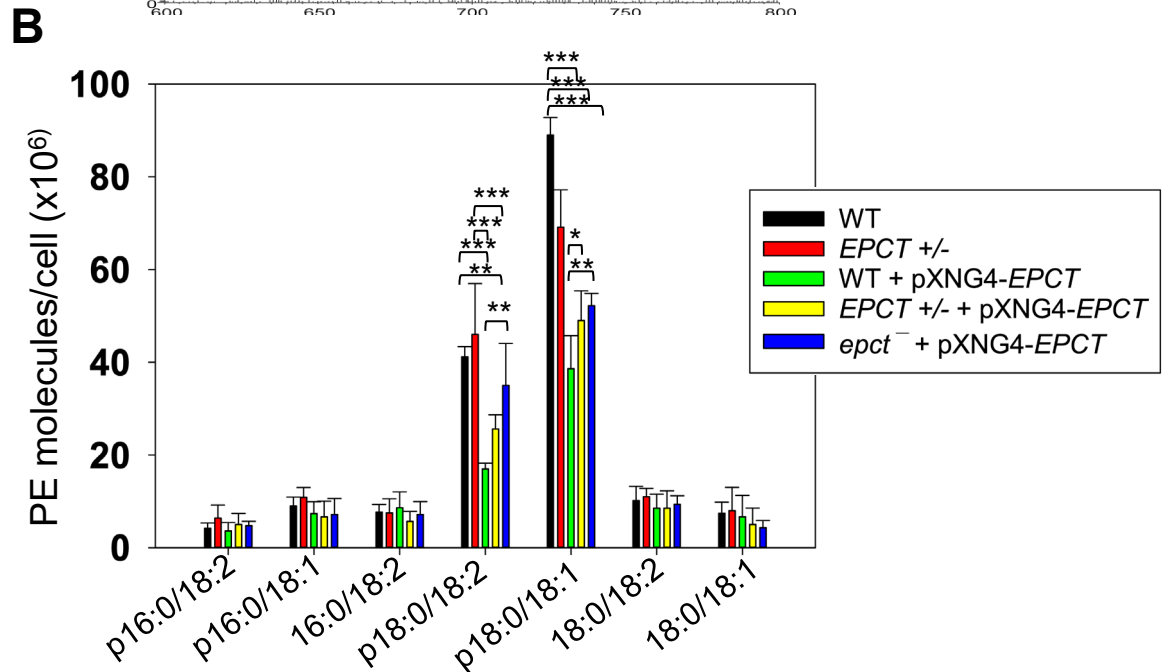
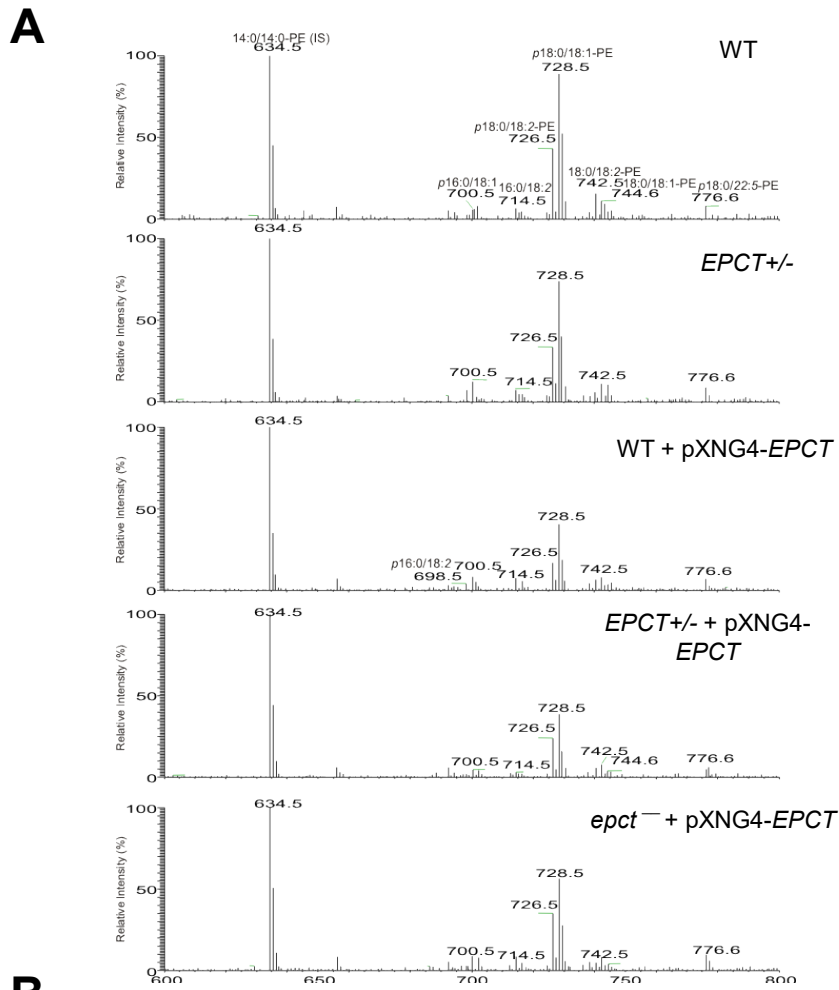
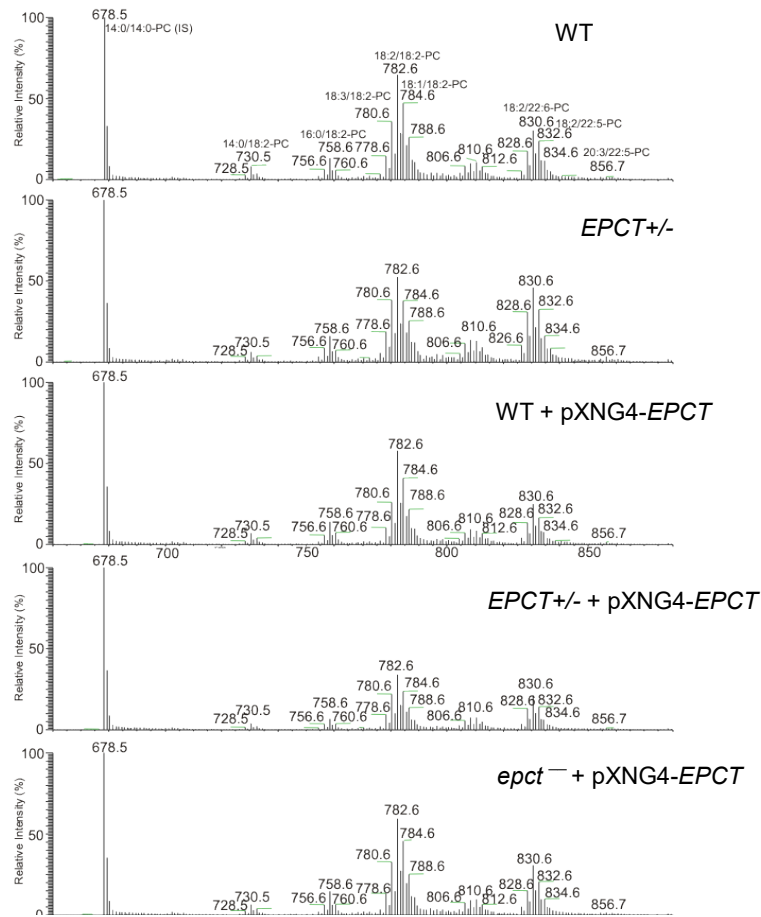


Fig. 8

A



B

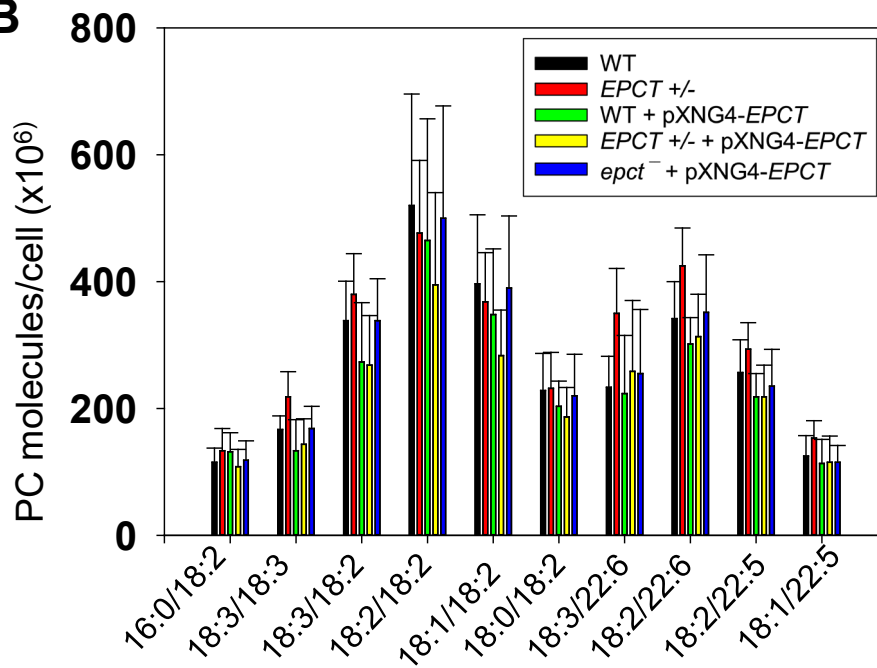
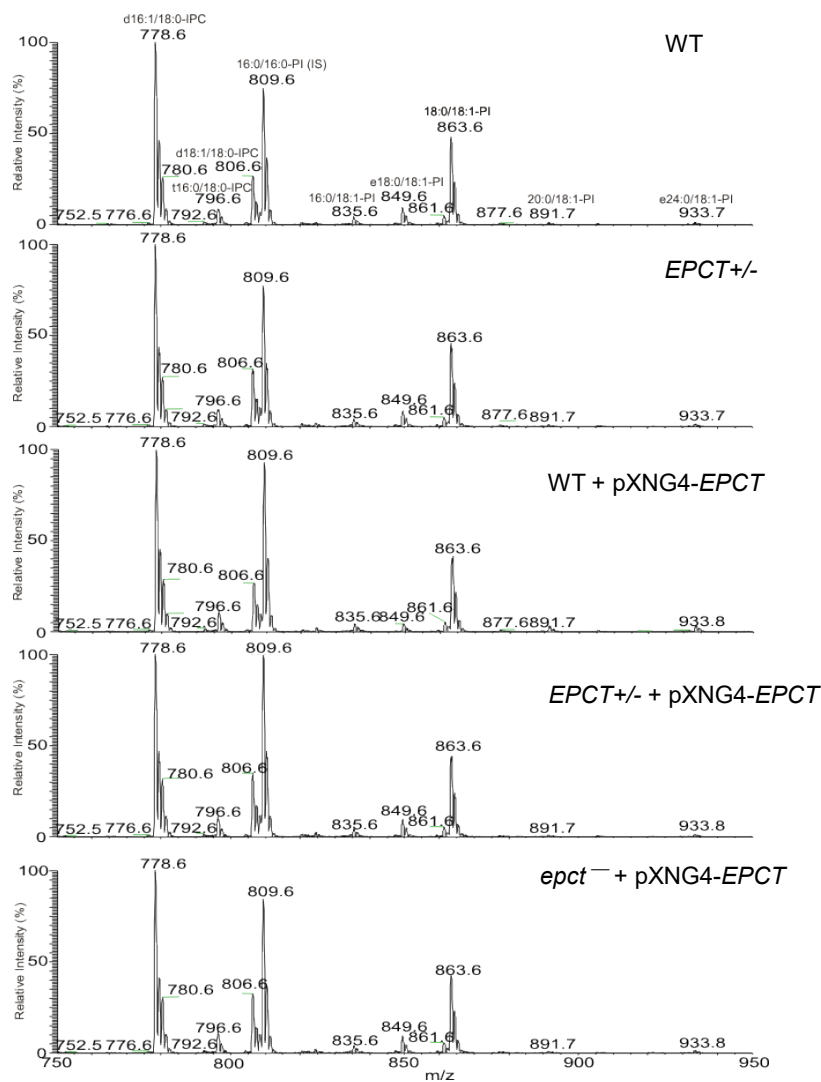


Fig. 9

A



B

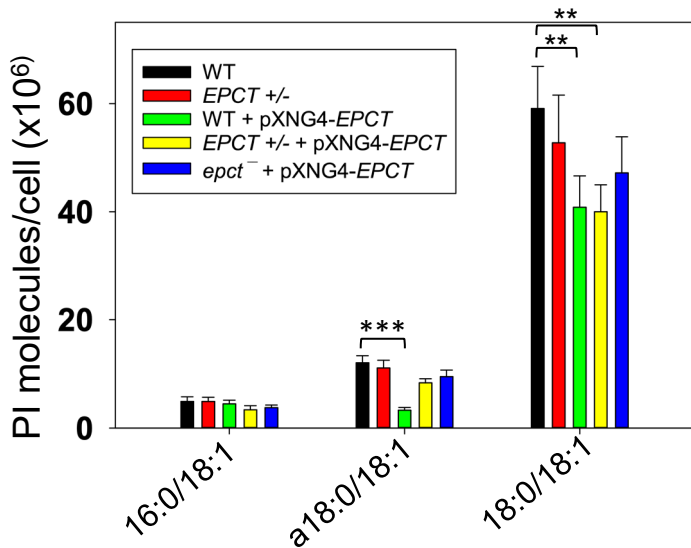


Fig. 10

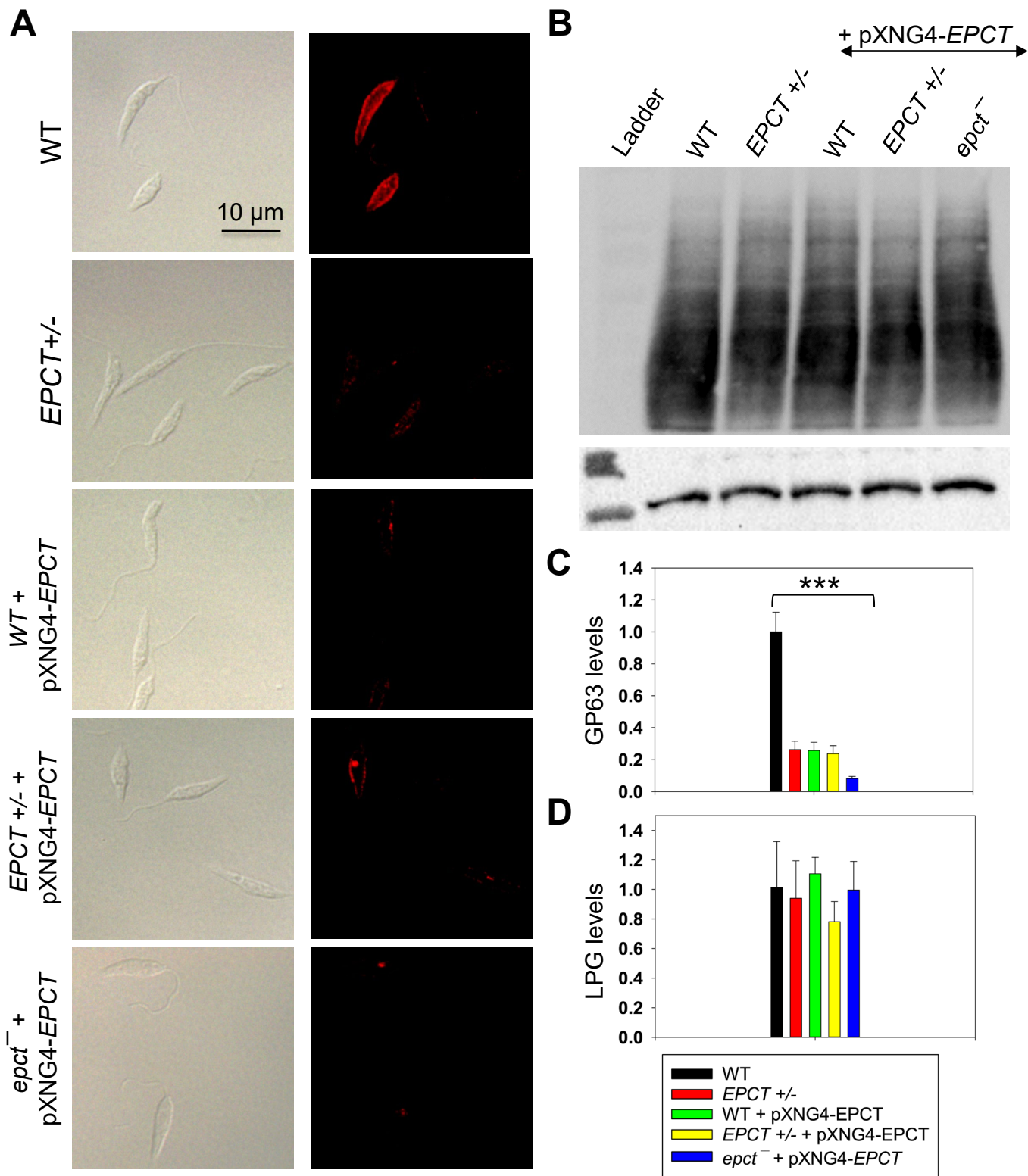
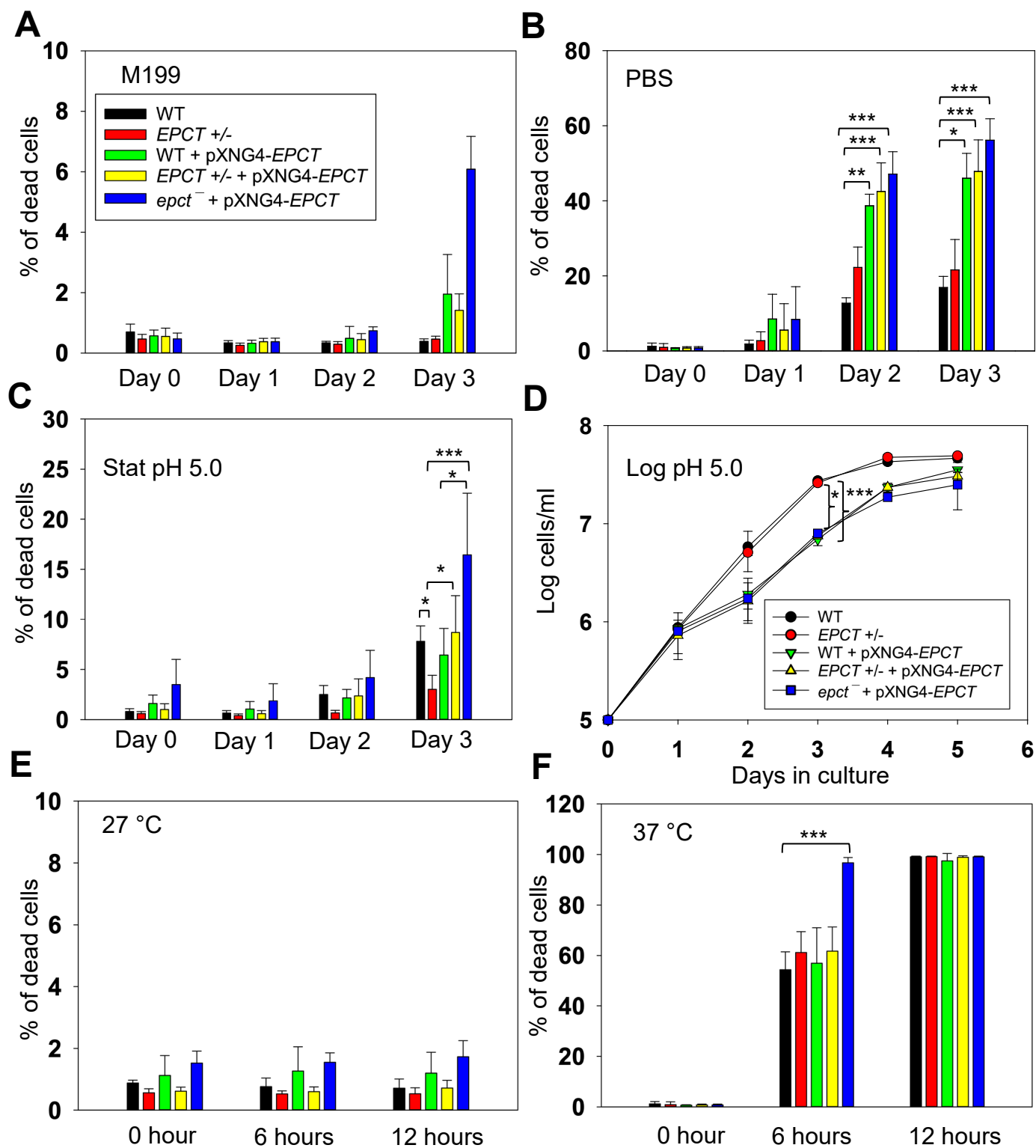


Fig. 11



Supplemental figures

Fig. S2

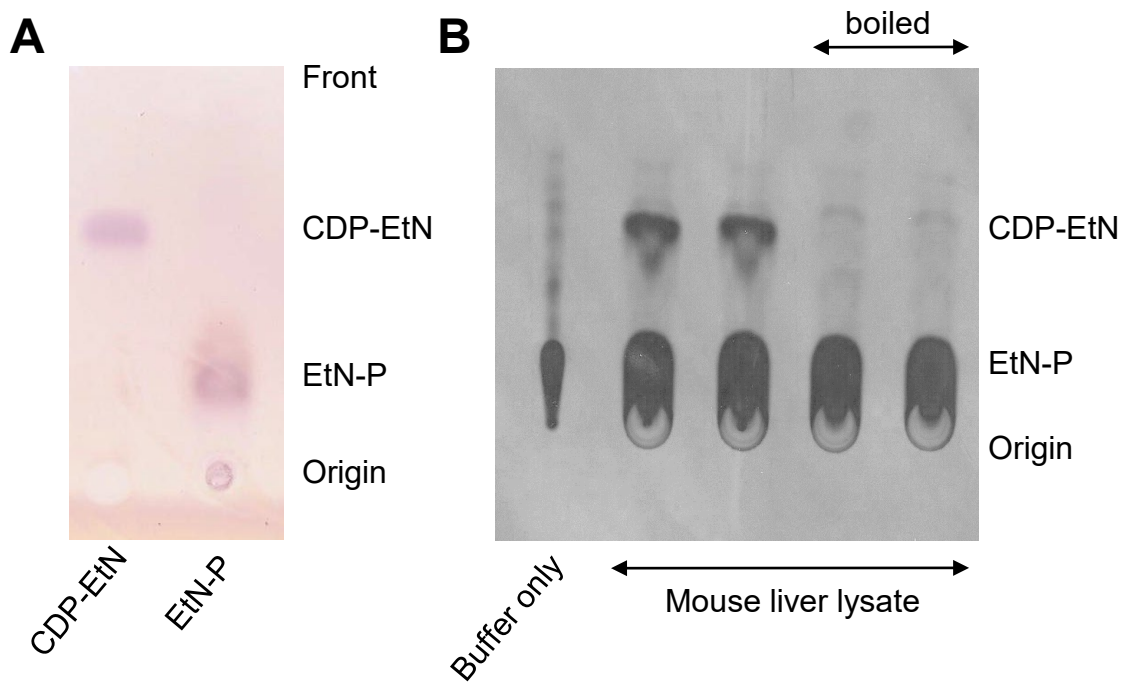


Fig. S3

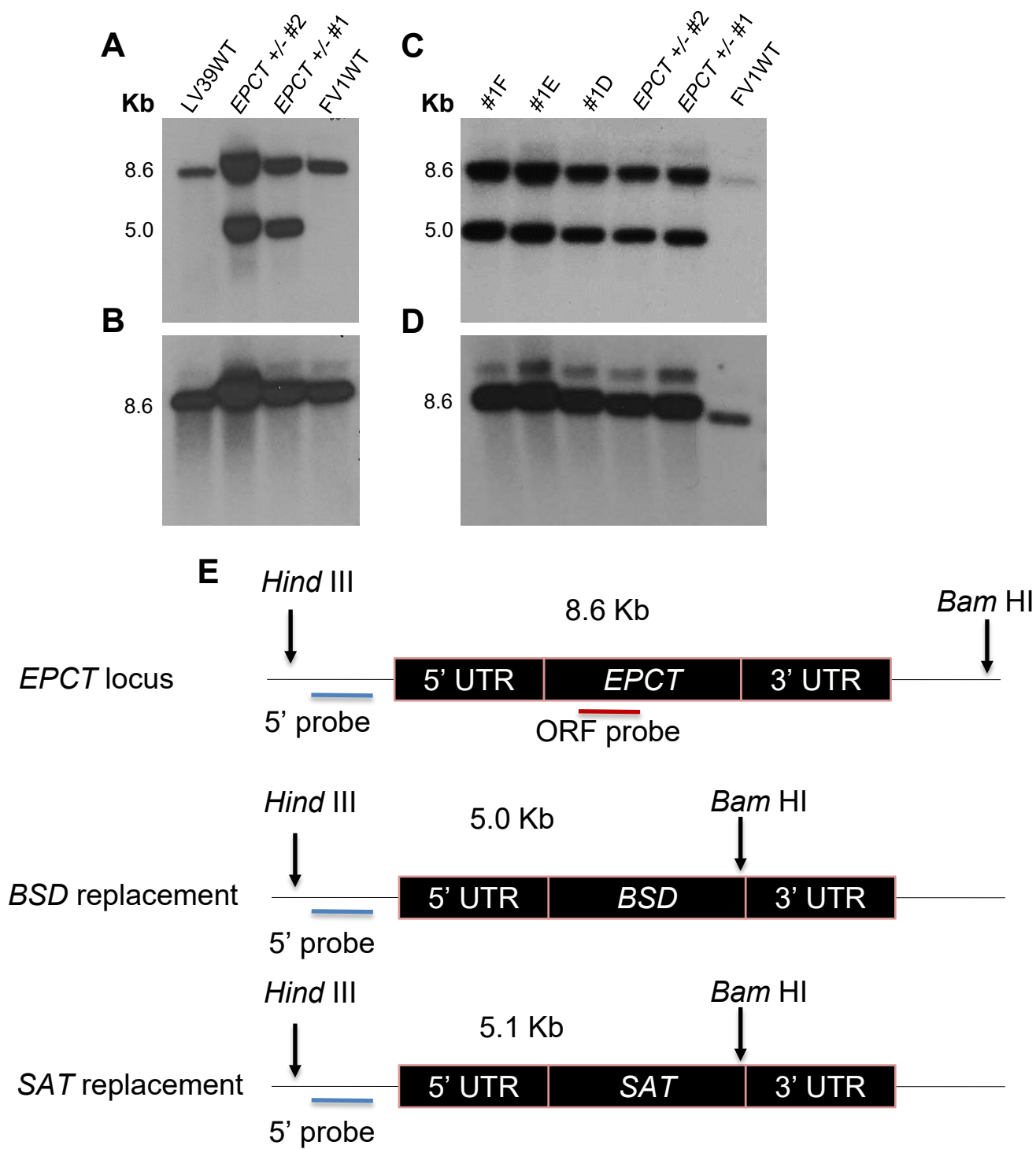


Fig. S4

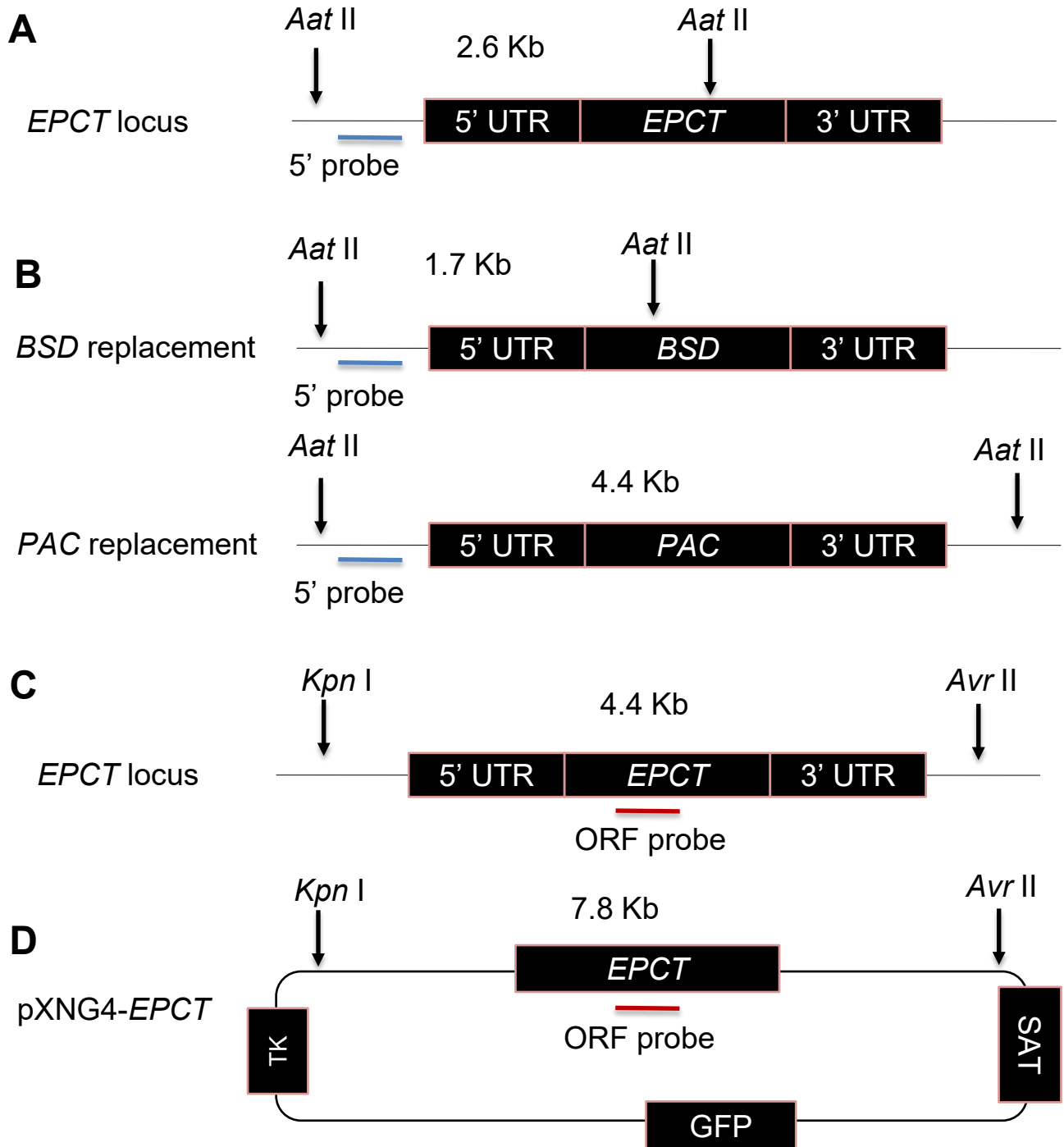


Fig. S6

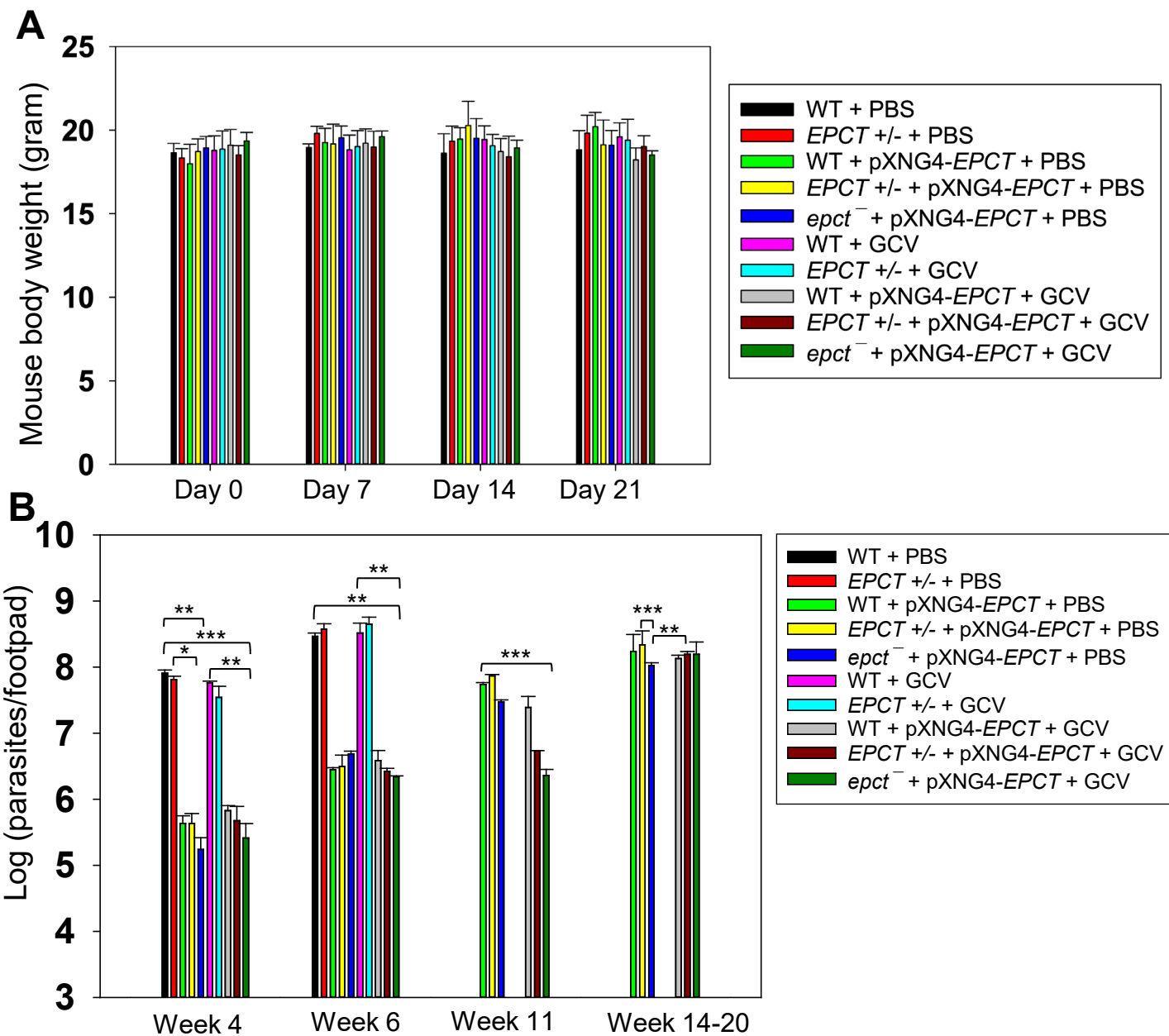
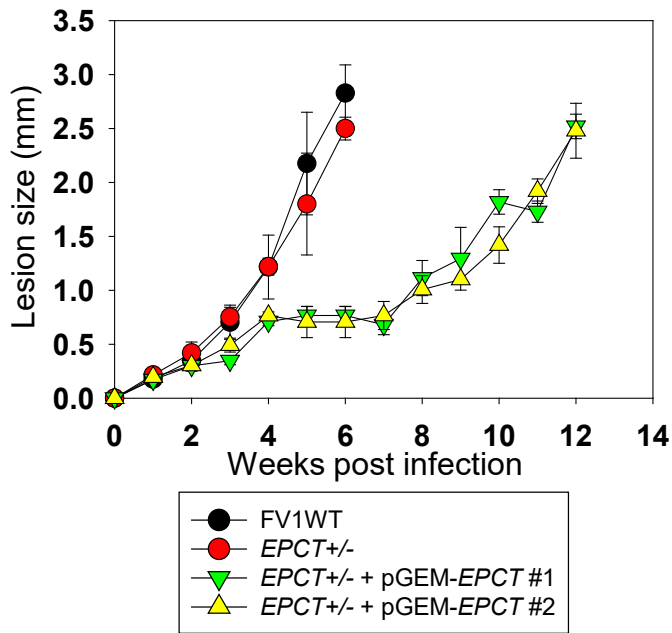


Fig. S7

A



B

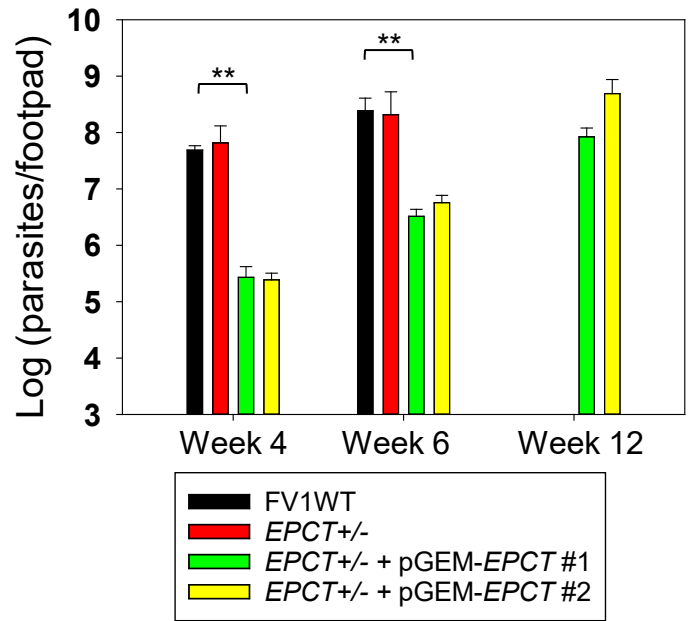


Fig. S8

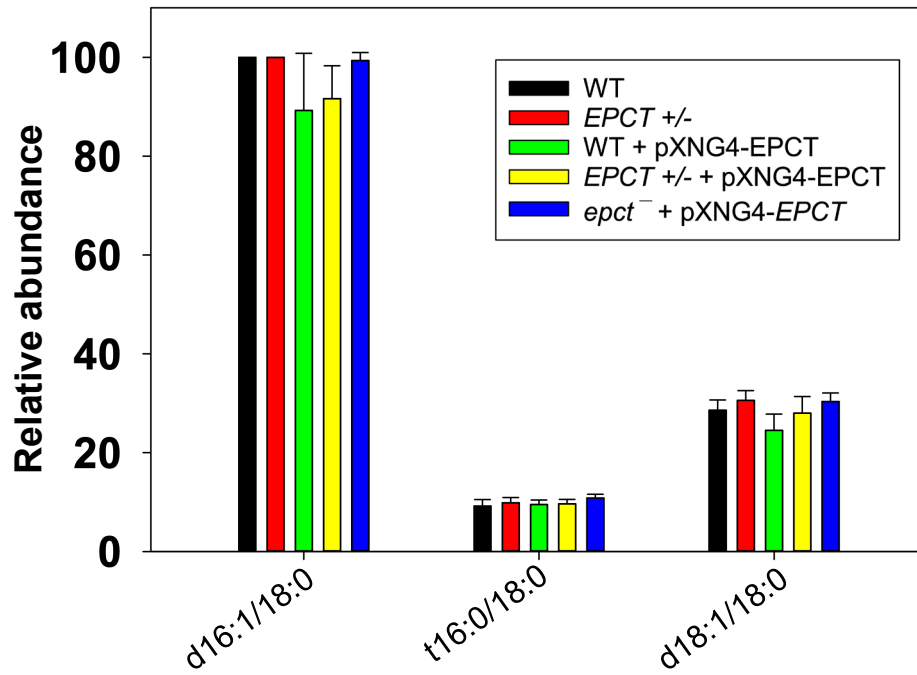


Fig. S9

